


Cite this: *CrystEngComm*, 2021, 23, 7576

Received 19th August 2021,
Accepted 4th October 2021

DOI: 10.1039/d1ce01113h

rsc.li/crystengcomm

Exploring covalent organic frameworks with new linkages is regarded as an efficient method to modulate the corresponding properties, and a new linkage is essential to the progress of this field. Herein, condensation of 1,3,5-triformylphloroglucinol with 1,1'-(1,4-phenylene)bis(thiourea), 1,1'-(2,5-dimethyl-1,4-phenylene)bis(thiourea) or 1,1'-(3,3'-dimethyl-[1,1'-biphenyl]-4,4'-diyl)bis(thiourea) were applied to construct COFs with thiourea linkages for the first time.

Covalent organic frameworks (COFs) are a novel class of crystalline porous polymers with structural periodicity and inherent porosity connected by strong covalent bonds.^{1,2} Owing to the great progress in the reticular chemistry of COFs, COFs have exhibited wide applications in gas adsorption,³ catalysis,⁴ energy storage,⁵ ion conductors,⁶ semiconductors,⁷ and sensors.⁸ Discovering new linkages for synthesizing COFs is a powerful way to tune their corresponding chemical and physical properties, which is of critical importance for the further advancement of this field but remains challenging. In particular, developing COFs based on new flexible linkages with highly crystallinity and porosity is a significant challenge as well.⁹

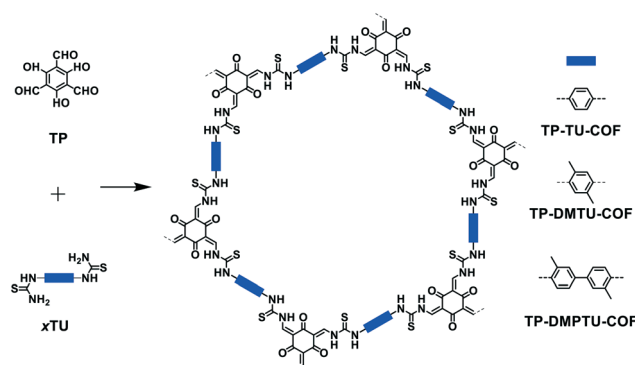
In 2018, Yaghi and coworkers synthesized two COFs with a flexible urea linkage, which have good crystallinity and porosity activated by methanol vapor. Herein, by replacing oxygen with sulfur in the linkage, we have synthesized three two-dimensional (2D) COFs based on flexible thiourea linkages with high crystallinity, high porosity, and robust chemical stability. We utilized 1,3,5-triformylphloroglucinol

Flexible thiourea linked covalent organic frameworks†

Baiwei Ma,^{‡a} Chunzhi Li,^{‡b} Lin Zhang,^a Lipeng Zhai,^{ib} *^a Fujia Hu,^a Yimeng Xu,^a Huijie Qiao,^a Zhuo Wang,^a Wenying Ai^a and Liwei Mi^{id} *^a

(TP) with 1,1'-(1,4-phenylene)bis(thiourea) (TU), 1,1'-(2,5-dimethyl-1,4-phenylene)bis(thiourea) (DMTU) or 1,1'-(3,3'-dimethyl-[1,1'-biphenyl]-4,4'-diyl)bis(thiourea) (DMPTU) to obtain a TP-TU-COF, TP-DMTU-COF, and TP-DMPTU-COF, respectively (Scheme 1). The corresponding COFs possess periodic one-dimensional pore channels with open thiourea active sites on the pore walls and thiourea linkages *via* their hydrogen bonding activation and can behave similarly to Lewis acids and be further used as heterogeneous catalysts. Therefore, we highlight the COFs in this study as efficient heterogeneous catalysts for Knoevenagel condensation.

We screened the reaction conditions including the solvents and reaction temperature for the condensation of TP with TU (Table S1†). According to the results, one significant feature is that the generation of crystalline frameworks is highly sensitive to the solvents and temperature (Fig. S1†). A TP-TU-COF with high crystallinity was synthesized with TP and TU in a mixed solvent of *N*-methyl-2-pyrrolidinone (NMP) and 1,2,4-trichlorobenzene (TCB) catalysed by 6 M aqueous acetic acid at 150 °C. Similarly, a TP-DMTU-COF and a TP-DMPTU-COF with high crystallinity were obtained under the same conditions.



Scheme 1 Schematic representation of the synthesis of the flexible thiourea-linked TP-TU-COF, TP-DMTU-COF, and TP-DMPTU-COF.

^a Henan Key Laboratory of Functional Salt Materials, Center for Advanced Materials Research, School of Material and Chemical Engineering, Zhongyuan University of Technology, Zhengzhou 45007, P. R. China.
E-mail: zhailp@zut.edu.cn, mhwzzu@163.com

^b State Key Laboratory of Catalysis, Dalian Institute of Chemical Physics, Chinese Academy of Science, 457 Zhongshan Road, Dalian 116023, China

† Electronic supplementary information (ESI) available. See DOI: 10.1039/d1ce01113h

‡ B. Ma and C. Li contributed to this work equally.

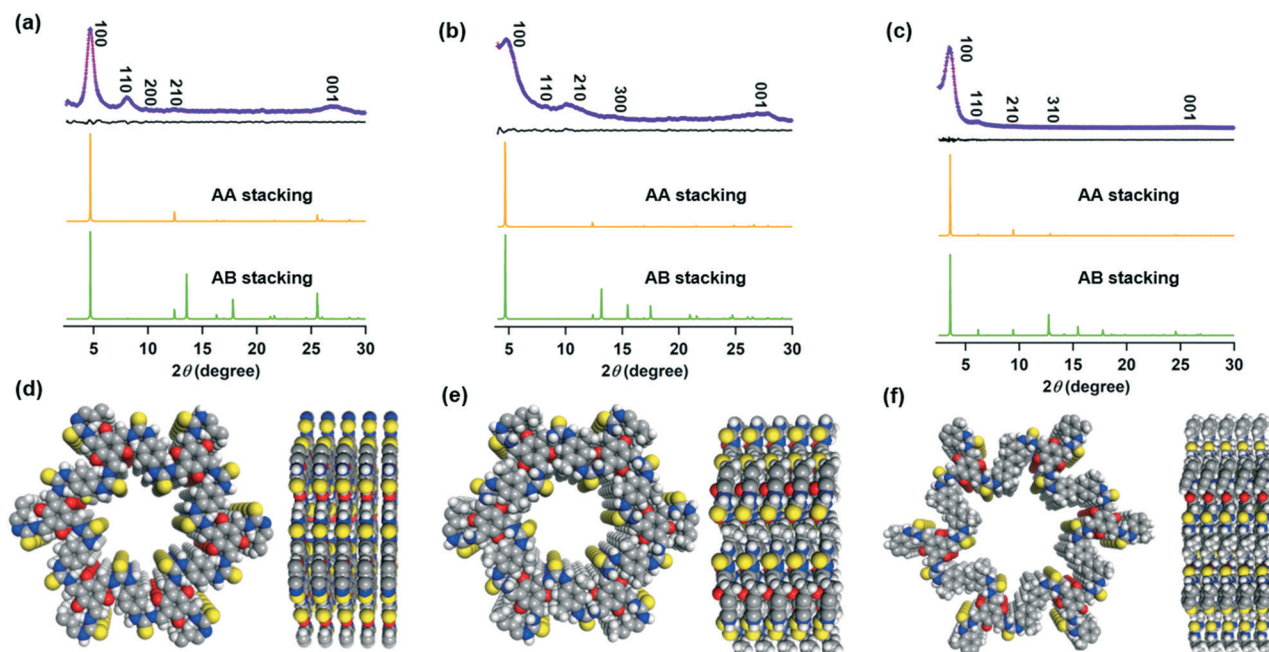


Fig. 1 PXRD patterns of the (a) TP-TU-COF, (b) TP-DMTU-COF, and (c) TP-DMPTU-COF: experimental (red) and Pawley refined (purple) PXRD patterns and their corresponding difference (black), as well as the simulated patterns for the eclipsed AA stacking mode (orange) and the staggered (AB) layer stacking mode (green). Top and side views of the reproduced AA stacking crystal structure of the (d) TP-TU-COF, (e) TP-DMTU-COF, and (f) TP-DMPTU-COF (H, white; C, gray; N, blue; O, red; S, yellow).

The crystalline structures of these COFs were resolved by powder X-ray diffraction (PXRD) measurements. The TP-TU-COF exhibited strong XRD peaks at 4.66, 8.12, 9.40, 12.44, and 26.30°, which can be assigned to the 100, 110, 200, 210, and 001 facets, respectively (Fig. 1a, red curve). The TP-DMTU-COF showed five peaks with the most intensive one at 4.68° and the other four peaks at 8.10, 9.36, 14.02, and 26.66°, which were attributed to the 100, 110, 300, and 001 facets, respectively (Fig. 1b, red curve). The TP-DMPTU-COF displayed five peaks at 3.56, 6.16, 9.42, 12.86, and 26.42°, which were assigned to the 100, 110, 210, 310, and 001 facets, respectively (Fig. 1c, red curve). Pawley refinement simulation by using a self-consistent charge density functional tight binding (SCC-DFTB) method was utilized to evaluate the theoretical stacking structures of the COFs. For these COFs, the Pawley refinement yielded XRD patterns (Fig. 1a–c, purple curve) that are in good agreement with the experimentally observed patterns, as proven and demonstrated by their negligible difference (black curve). Besides, the peak position and intensity of the XRD pattern (Fig. 1a–c, orange curve) can be reproduced with the AA stacking mode, whereas the AB stacking mode generates the XRD pattern that largely deviates from the experimentally observed profiles (Fig. 1a–c, green curve, and Fig. S2–S4†). Moreover, Pawley refinement provided factors, which are in good agreement with the experimental PXRD data, for the TP-TU-COF ($R_{wp} = 4.47\%$ and $R_p = 3.44\%$), TP-DMTU-COF ($R_{wp} = 3.17\%$ and $R_p = 2.34\%$), and TP-DMPTU-COF ($R_{wp} = 5.36\%$ and $R_p = 2.77\%$). Fig. 1d–f demonstrate their AA stacking mode from top and side views.

The permanent porous structures of these COFs were investigated by nitrogen sorption analysis at 77 K. As shown

in Fig. 2a, the TP-TU-COF and TP-DMTU-COF exhibited typical type-I nitrogen sorption isotherms indicating their microporous structures. In contrast, a typical type-IV sorption isotherm was found for the TP-DMPTU-COF, which indicated a mesoporous structure (Fig. 2a, purple). The Brunauer–Emmett–Teller (BET) surface areas of the TP-TU-COF, TP-DMTU-COF and TP-DMPTU-COF were calculated to be 714.7 $\text{m}^2 \text{g}^{-1}$, 518.2 $\text{m}^2 \text{g}^{-1}$, and 1125.7 $\text{m}^2 \text{g}^{-1}$, respectively, which were much higher than those of the other reported COFs with flexible linkages to date. Non-local density functional theory (NLDFT) was applied to investigate the corresponding pore size distribution for these three COFs. The pore sizes of these three COFs were evaluated to be around 1.50, 1.59, and 2.1 nm (Fig. 2b), which are smaller than the theoretical values calculated from their AA stacking mode. The smaller pore sizes for these three COFs were attributed to their highly flexible linkage structures.

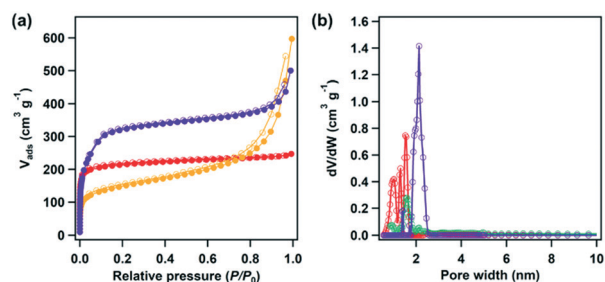


Fig. 2 (a) Nitrogen sorption isotherms at 77 K of the (red) TP-TU-COF, (orange) TP-DMTU-COF, and (purple) TP-DMPTU-COF. (b) Pore size distributions calculated using non-local density functional theory.

To understand the nature of the thiourea linkage and frameworks, Fourier transform infrared (FTIR) and ^{13}C cross polarization magic angle spinning (CP-MAS) NMR spectroscopy techniques were employed. As for FTIR, data were collected using the starting monomers and COF materials (Fig. S5†). The stretching vibration bands around 1582 and 1445 cm^{-1} were assigned to the $\text{C}=\text{O}$ and $\text{C}=\text{C}$ bonds, respectively, indicating the existence of the keto form of these COFs. Besides, the peaks around 3450–3170 and 1270 cm^{-1} were attributed to the N–H and $\text{C}=\text{S}$ groups, respectively. Finally, the peak at 2925 cm^{-1} was attributed to the CH_3 groups of the TP-DMTU-COF and TP-DMPTU-COF. CP-MAS ^{13}C solid-state NMR spectroscopy further confirmed these groups over the COF networks (Fig. S6–S8†). Taking the TP-DMPTU-COF as an example, the peaks at 15, 181, 184, and 187 ppm were attributed to the carbon of CH_3 , C–N, $\text{C}=\text{S}$, and $\text{C}=\text{O}$, respectively (Fig. S8†). The peaks from 100 to 150 ppm were attributed to the carbons of aromatic networks. The elemental analysis results for these three COFs are in good agreement with the theoretical values of their infinite 2D sheet (Table S2†). Thermal gravimetric analysis (TGA) of these three COFs exhibits an obvious two-stage weight loss at 200–400 $^{\circ}\text{C}$ and above 400 $^{\circ}\text{C}$. The degradation of flexible thiourea linkages is responsible for the initial weight loss, and the second loss is attributed to the decomposition of the COF networks (Fig. S9†). Field-emission scanning electron microscopy (FE-SEM) revealed that the TP-TU-COF adopts a micrometer-scale sphere-like morphology, whereas the TP-DMTU-COF and TP-DMPTU-COF exhibit a fiber-like morphology (Fig. S10†). EDX mapping of these three COFs demonstrated that the elemental distribution was uniform over the networks (Fig. S11–S13†). High-resolution transmission electron microscopy (HR-TEM) was performed to further investigate the periodic structures of these COFs (Fig. S14–S16†). For example, as shown in Fig. S16a and b,† a honeycomb-like hexagonal porous structure was obviously observed in the 001 direction for the TP-DMPTU-COF. An obvious layered structure of parallel sheets was found for the TP-DMPTU-COF in Fig. S16c.†

Chemical stability toward different solvents is a key factor for further exploring COFs' applications. The stability of these COFs was investigated by dispersing the sample in strong acid and base for 24 h, and then their PXRD profiles were evaluated after vacuum drying for 12 h. As shown in Fig. S17,† there is no obvious change in the PXRD peak position and intensity after treatment in 1 M HCl and 1 M NaOH for 24 h. With their excellent crystallinity, high BET surface area, and abundant thiourea catalytic active sites, these three thiourea-linked COFs were further applied as heterogeneous catalysts for Knoevenagel reactions.

As shown in Table S3,† to evaluate the catalytic activities of the as-prepared COFs, Knoevenagel condensation reactions between 4-chlorobenzaldehyde (**1a**) and malononitrile were conducted. We firstly investigated the background reaction situation without the COFs in toluene, and only the trace product was found. After screening the reaction solvents,

97%, 95%, and 98% yields were achieved for the TP-TU-COF, TP-DMTU-COF, and TP-DMPTU-COF, respectively (entry 8, 9, and 10, Table S3†). Therefore, the TP-TU-COF, TP-DMTU-COF, and TP-DMPTU-COF materials can catalyze the reaction smoothly. Then the catalytic activities of the TP-DMPTU-COF were further investigated *via* expanding the substrate scopes ranging from electron-withdrawing and electron-donating groups to heterocycles (Fig. 3, 2a–2l). Firstly, aromatic aldehydes with weak electron-withdrawing halogen groups on the phenyl ring were applied to evaluate the performance of the TP-DMPTU-COF as a catalyst, and excellent yields (92–98%, 2a–2d) were obtained. In addition, 97% yield was achieved for compound **2i** with two chloro groups. Furthermore, compound 4-nitrobenzaldehyde (**1e**) with a strong electron-withdrawing nitro group on the phenyl ring can give 89% yield at 40 $^{\circ}\text{C}$, whereas only 71% yield was obtained at a higher temperature of 60 $^{\circ}\text{C}$. This lower yield at higher temperature is because the activity of substrate **1e** is very high for the Knoevenagel reaction. In this respect, lower temperature favors the reaction selectivity to avoid the production of side products compared with higher temperature. Aromatic aldehyde **1f** without any substituent on the phenyl ring gave the **2f** product in 99% yield in this case. Finally, we also investigated the performance of the TP-DMPTU-COF when the substrates have methyl and methoxy electron-donating groups on the phenyl ring. Similarly, excellent yields were obtained (**2g** and **2h**). Except for

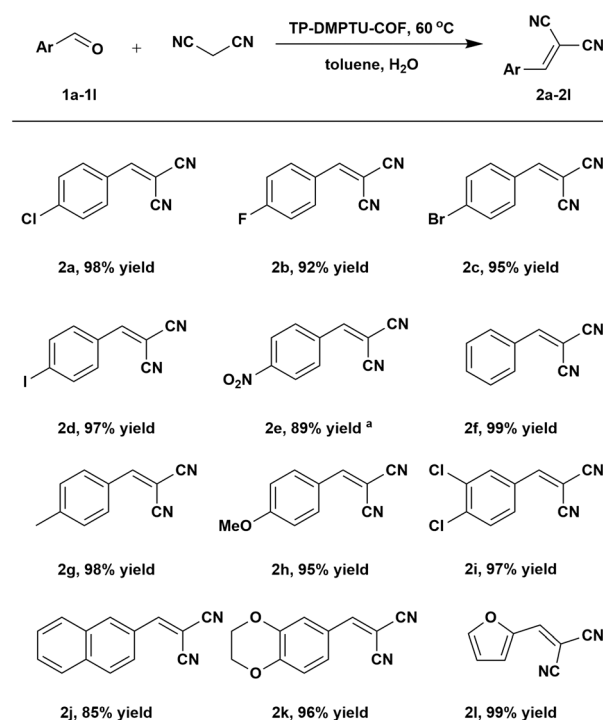


Fig. 3 Substrate scope of the Knoevenagel condensation reaction. Unless otherwise noted, the reaction was performed with 2 mol% of the TP-DMPTU-COF (7.8 mg), aldehydes (0.3 mmol) and malononitrile (0.45 mmol, 1.5 equiv) in toluene: H_2O (2.0 ml: 0.4 ml) at 60 $^{\circ}\text{C}$ for 10 h; yield of the isolated product. ^aThe reaction was conducted at 40 $^{\circ}\text{C}$.

benzene ring compounds, naphthalene nucleus product **2j** was obtained with a slight decrease in 85% yield. It was worth mentioning that other types of substrates such as 2,3-dihydrobenzo[*b*][1,4]dioxine-6-carbaldehyde and furfuraldehyde respectively gave the **2k** and **2l** products in 96% and 99% yields. To investigate the catalytic recycling performance of the TP-DMPTU-COF, we continuously proceeded the reaction of **1a** with malononitrile for five cycles (Fig. S18†). The catalytic activity of the TP-DMPTU-COF was retained after five cycles, and an obvious change of the PXRD pattern was not found, which indicated that it can be used as an efficient, stable and recyclable heterogeneous catalyst (Fig. S19†).

In conclusion, we have designed and synthesized three COFs based on highly flexible thiourea linkages with excellent porosity, crystallinity, and chemical stability toward harsh conditions. A thiourea linkage was employed to construct COF materials for the first time. The abundant thiourea groups uniformly distributed on the pore channels can be utilized as activation sites for efficiently catalyzing the organic reactions. Notably, these COFs exhibited excellent catalytic performance, ignoring the substrate categories, and the COF materials can be recycled. Therefore, we believed that our work provides a new window into COF synthesis chemistry and its potential application in heterogeneous catalysis.

Author contributions

Baiwei Ma: experiment implementation and guidance, data collection and sorting. Chunzhi Li: software, calculation and data test. Lin Zhang, Fujia Hu, Yimeng Xu, Huijie Qiao, Zhuo Wang and Wenying Ai: experiment implementation. Baiwei Ma, Lipeng Zhai and Liwei Mi discussed the results and prepared the manuscript.

Conflicts of interest

There are no conflicts to declare.

Acknowledgements

This work was supported by the National Natural Science Foundation of China (Grants U1804126, U1804129, 21671205 and 21771164) and the Support Program of Science and Technology Innovation Leading Talent of Zhongyuan (Grant 204200510014). L. Zhai appreciates support from the National Natural Science Foundation of China (No. 52103277), the Key Projects of Science and Technology of Henan Province (No. 212102210208), and the Zhongyuan University of Technology start-up grant. L. Zhang thanks the support from the Zhongyuan University of Technology (K2019QN001).

Notes and references

- (a) A. P. Côté, A. I. Benin, N. W. Ockwig, M. O'Keeffe, A. J. Matzger and O. M. Yaghi, *Science*, 2005, **310**, 1166; (b) Z. Wang, S. Zhang, Y. Chen, Z. Zhang and S. Ma, *Chem. Soc. Rev.*, 2020, **49**, 708; (c) L. Zhang, Y. Zhou, M. Jia, Y. He, W. Hu, Q. Liu, J. Li, X. Xu, C. Wang, A. Carisson, S. Lazar, A. Meingast, Y. Ma, J. Xu, W. Wen, Z. Liu, J. Cheng and H. Deng, *Matter*, 2020, **2**, 1049; (d) S. Tao and D. Jiang, *CCS Chem.*, 2021, **3**, 2003; (e) P. Shao, J. Li, F. Chen, L. Ma, Q. Li, M. Zhang, J. Zhou, A. Yin, X. Feng and B. Wang, *Angew. Chem., Int. Ed.*, 2018, **57**, 16501.
- (a) K. Wang, Z. Jia, Y. Bai, X. Wang, S. E. Hodgkiss, L. Chen, S. Y. Chong, X. Wang, H. Yang, H. Xu, F. Feng, J. W. Ward and A. I. Cooper, *J. Am. Chem. Soc.*, 2020, **142**, 11131; (b) Y. Wang, H. Liu, Q. Pan, C. Wu, W. Hao, J. Xu, R. Chen, J. Liu, Z. Li and Y. Zhao, *J. Am. Chem. Soc.*, 2020, **142**, 5958; (c) C. Gao, J. Li, S. Yin, J. Sun and C. Wang, *J. Am. Chem. Soc.*, 2020, **142**, 3718; (d) R.-R. Liang, R.-H. A, S.-Q. Xu, Q.-Y. Qi and X. Zhao, *J. Am. Chem. Soc.*, 2020, **142**, 70; (e) P.-L. Wang, S.-Y. Ding, Z.-C. Zhang, Z.-P. Wang and W. Wang, *J. Am. Chem. Soc.*, 2019, **141**, 18004; (f) Y. Li, L. Guo, Y. Lv, Z. Zhao, Y. Ma, W. Chen, G. Xing, D. Jiang and L. Chen, *Angew. Chem., Int. Ed.*, 2021, **60**, 5363.
- (a) Y. Yusran, X. Guan, H. Li, Q. Fang and S. Qiu, *Natl. Sci. Rev.*, 2020, **7**, 170; (b) J. L. Fenton, D. W. Burke, D. Qian, M. O. D. L. Cruz and W. R. Dichtel, *J. Am. Chem. Soc.*, 2021, **143**, 1466; (c) C. Zhao, H. Lyu, Z. Ji, C. Zhu and O. M. Yaghi, *J. Am. Chem. Soc.*, 2020, **142**, 14450; (d) S. An, Q. Xu, Z. Ni, J. Hu, C. Peng, L. Zhai, Y. Guo and H. Liu, *Angew. Chem., Int. Ed.*, 2021, **60**, 9959; (e) L. Zhai, N. Huang, H. Xu, Q. Chen and D. Jiang, *Chem. Commun.*, 2017, **53**, 4242; (f) Y. Li, Q. Wu, X. Guo, M. Zhang, B. Chen, G. Wei, X. Li, X. Li, S. Li and L. Ma, *Nat. Commun.*, 2020, **11**, 599.
- (a) C. Qian, W. Zhou, J. Qiao, D. Wang, X. Li, W. L. Teo, X. Shi, H. Wu, J. Di, H. Wang, G. Liu, L. Gu, J. Liu, L. Feng, Y. Liu, S. Quek, K. P. Loh and Y. Zhao, *J. Am. Chem. Soc.*, 2020, **142**, 18138; (b) N. Huang, K. H. Lee, Y. Yue, X. Xu, S. Irle, Q. Jiang and D. Jiang, *Angew. Chem., Int. Ed.*, 2020, **59**, 16587; (c) C. Yuan, S. Fu, K. Yang, B. Hou, Y. Liu, J. Jiang and Y. Cui, *J. Am. Chem. Soc.*, 2021, **143**, 369; (d) Y. Qian, D. Li, Y. Han and H.-L. Jiang, *J. Am. Chem. Soc.*, 2020, **142**, 20763; (e) M. Lu, M. Zhang, C.-G. Liu, J. Liu, L.-J. Shang, M. Wang, J.-N. Chang, S.-L. Li and Y.-Q. Lan, *Angew. Chem., Int. Ed.*, 2021, **60**, 4864–4871.
- (a) Y. Yusran, Q. Fang and V. Valtchev, *Adv. Mater.*, 2020, **32**, 2002038; (b) S. Wang, Q. Wang, P. Shao, Y. Han, X. Gao, L. Ma, S. Yuan, X. Ma, J. Zhou, X. Feng and B. Wang, *J. Am. Chem. Soc.*, 2017, **139**, 4258; (c) E. Vitaku, C. N. Gannett, K. L. Carpenter, L. Shen, H. D. Abruna and W. R. Dichtel, *J. Am. Chem. Soc.*, 2020, **142**, 16; (d) A. Halder, M. Ghosh, A. K. M. S. Bera, M. Addicoat, H. S. Sasmal, S. Karak, S. Kurungot and R. Banerjee, *J. Am. Chem. Soc.*, 2018, **140**, 10941; (e) C. Gao, J. Li, S. Yin, J. Sun and C. Wang, *Nat. Commun.*, 2020, **11**, 4919.
- (a) S. Tao, L. Zhai, A. D. D. Wananke, M. A. Addicoat, Q. Jiang and D. Jiang, *Nat. Commun.*, 2020, **11**, 1981; (b) Q. Xu, S. Tao, Q. Jiang and D. Jiang, *Angew. Chem., Int. Ed.*, 2020, **59**, 4557; (c) Z. Guo, Y. Zhang, D. Yu, J. Li, S. Li, P. Shao, X. Feng and B. Wang, *J. Am. Chem. Soc.*, 2019, **141**,

- 1923; (d) X. Wu, Y.-L. Hong, B. Xu, Y. Nishiyama, W. Jiang, J. Zhu, G. Zhang, S. Kitagawa and S. Horike, *J. Am. Chem. Soc.*, 2020, **142**, 14357; (e) L. Liu, L. Yin, D. Cheng, S. Zhao, H.-Y. Zhang, N. Zhang and G. Zhu, *Angew. Chem., Int. Ed.*, 2021, **60**, 14875.
- 7 (a) E. Jin, J. Li, K. Geng, Q. Jiang, H. Xu, Q. Xu and D. Jiang, *Nat. Commun.*, 2018, **9**, 4143; (b) H. Ding, J. Li, G. Xie, G. Lin, R. Chen, Z. Peng, C. Yang, B. Wang, J. Sun and C. Wang, *Nat. Commun.*, 2018, **9**, 15234; (c) J. Xu, C. Yang, S. Bi, W. Wang, Y. He, D. Wu, Q. Liang, X. Wang and F. Zhang, *Angew. Chem., Int. Ed.*, 2020, **59**, 23845; (d) W. Chen, L. Wang, D. Mo, F. He, Z. Wen, X. Wu, H. Xu and L. Chen, *Angew. Chem., Int. Ed.*, 2020, **59**, 16902.
- 8 (a) Y. Ma, Y. Wang, H. Li, X. Guan, B. Li, M. Xue, Y. Yan, V. Valtchev, S. Qiu and Q. Fang, *Angew. Chem., Int. Ed.*, 2020, **59**, 19633; (b) X. Liu, J. Li, B. Gui, G. Lin, Q. Fu, S. Yin, X. Liu, J. Sun and C. Wang, *J. Am. Chem. Soc.*, 2021, **143**, 2123; (c) L. Grunenberg, G. Savasci, M. W. Terban, V. Duppei, I. Moudrakovski, M. Etter, R. E. Dinnebier, C. Ochsenfeld and B. V. Lotsch, *J. Am. Chem. Soc.*, 2021, **143**, 3430; (d) F. Yu, W. Liu, S.-W. Ke, M. Kurmoo, J.-L. Zuo and Q. Zhang, *Nat. Commun.*, 2020, **11**, 5534; (e) X. L. Li, *Mater. Chem. Front.*, 2021, **5**, 2931.
- 9 (a) S. Jiang, L. C. Meng, W. Y. Ma, G. C. Pan, W. Zhang, Y. C. Zou, L. J. Liu, B. Xu and W. J. Tian, *Mater. Chem. Front.*, 2021, **5**, 4193; (b) C. Zhao, C. S. Diercks, C. Zhu, N. Hanikel, X. Pei and O. M. Yaghi, *J. Am. Chem. Soc.*, 2018, **140**, 16438; (c) B. Zhang, M. Wei, H. Mao, X. Pei, S. A. Alshimmri, J. A. Reimer and O. M. Yaghi, *J. Am. Chem. Soc.*, 2018, **140**, 12715; (d) S. Bi, C. Yang, W. Zhang, J. Xu, L. Liu, D. Wu, X. Wang, Y. Han, Q. Liang and F. Zhang, *Nat. Commun.*, 2019, **10**, 2467; (e) E. Jin, M. Asada, Q. Xu, S. Dalapati, M. A. Addicoat, M. A. Brady, H. Xu, T. Nakamura, T. Heine, Q. Chen and D. Jiang, *Science*, 2017, **357**, 673.

Supporting Information

Flexible Thiourea Linked Covalent Organic Frameworks

Baiwei Ma,^{a+} Chunzhi Li,^{b+} Lipeng Zhai,^{a*} Fujia Hu,^a Yimeng Xu,^a Huijie Qiao,^a Zhuo Wang,^a Wenying Ai,^a Liwei Mi^{a*}

a: Henan Key Laboratory of Functional Salt Materials, Center for Advanced Materials Research, School of Material and Chemical Engineering, Zhongyuan University of Technology, Zhengzhou 450007 (P. R. China)

b: State Key Laboratory of Catalysis, Dalian Institute of Chemical Physics, Chinese Academy of Science, 457 Zhongshan Road, Dalian 116023 (P. R. China)

Email: zhailp@zut.edu.cn, mlwzzu@163.com

Contents

Section A. Materials and Methods

Section B. Supporting Figures

Section C. Supporting Tables

Section D. Supporting References

Section A. Materials and Methods

^1H NMR and ^{13}C NMR spectra were measured on a Bruker 400 MHz spectrometer, while chemical shifts (δ in ppm) were determined using a standard of the solvent residual proton. Solid state Fourier ^{13}C NMR spectra were measured on a Bruker 400 MHz spectrometer. Transform infrared (FT IR) spectra were recorded on a JASCO model FT IR-6100 infrared spectrometer. X-ray diffraction (XRD) data were recorded on a Bruker D8 Focus Powder X-ray Diffractometer by using powder on glass substrate, from $2\theta = 2^\circ$ up to 30° with 0.01° increment. Elemental analysis was performed on an Elementar vario MICRO cube elemental analyzer. TGA measurements were performed on a Discovery TGA under N_2 , by heating from 30 to 800°C at a rate of $10^\circ\text{C min}^{-1}$. Nitrogen sorption isotherms were measured at 77 K with a TriStar II instrument (Micromeritics). The Brunauer-Emmett-Teller (BET) method was utilized to calculate the specific surface areas. By using the non-local density functional theory (NLDF) model, the pore volume was derived from the sorption curve. Morphology images were characterized with a Zeiss Merlin Compact field emission scanning electron microscope (FE-SEM) equipped with an energy-dispersive X-ray spectroscopy (EDS) system at an electric voltage of 5 KV. HRTEM images were obtained with a transmission electron microscope (TEM, FEI Tecnai G2) installed with an energy dispersive spectrometer (EDS, Oxford).

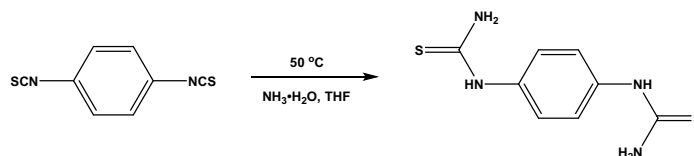
Simulations. The process of simulating COF structure was accomplished via Materials Studio software (version 8.0) of Accelrys Company. The hexagonal crystal system with P6 symmetry group was set as the initial AA stacking COFs structures. The cell parameters a and c were obtained from the calculation of experimental PXRD of COF by Bragg's law. After the smallest asymmetric unit was filled into the blank cell, the Forcite tools package was employed to optimize the cell geometry including energy minimization. The AB stacking structure was built with the similar process as described above, with the exception that a supercell with double c value was selected as the initial cell of staggered structure. The cell optimized from the universal force fields was subsequently refined using the Pawley refinement method in Reflex tools.^[S1-S3]

Stability test. COF samples (20 mg) were kept for 24h at room temperature in HCl (1 M), and NaOH (1 M), respectively. The samples were collected by filtration and rinsed with water and THF several times. The COF were dried under vacuum at 100°C for 12 h and subjected to PXRD.

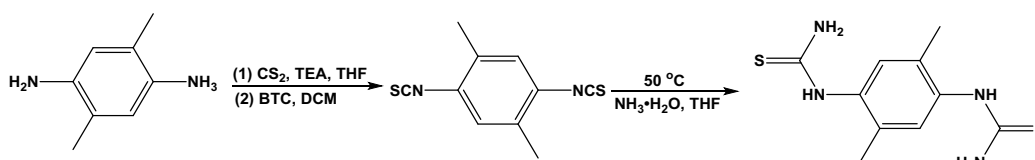
Materials: 1,4-Phenylene diisocyanate, anhydrous N-methyl-2-pyrrolidinone (NMP), 1,2,4-trichlorobenzene (TCB), triethylamine (TEA), and ammonium hydroxide (28–30%) were purchased from Sigma Aldrich. The acetic acid, 1,2-dichloromethane (DCM), N, N-diethylformamide (DEF), Tetrahydrofuran (THF), acetone and CS_2 were purchased from Aladdin Chemicals. 1,3,5-Triformylphloroglucinol (TP) was purchased from Shanghai zhuogao new material Co., Ltd. 1,1'-(1,4-phenylene) bis(thiourea) (TU), 1,1'-(2,5-dimethyl-1,4-phenylene) bis(thiourea) (DMTU) and 1,1'-(3,3'-

dimethyl-[1,1'-biphenyl]-4,4'-diyl) bis(thiourea) (DMPTU) were prepared by ourselves, All the other solvents were purchased from Aladdin Chemicals and used as received without further purification.

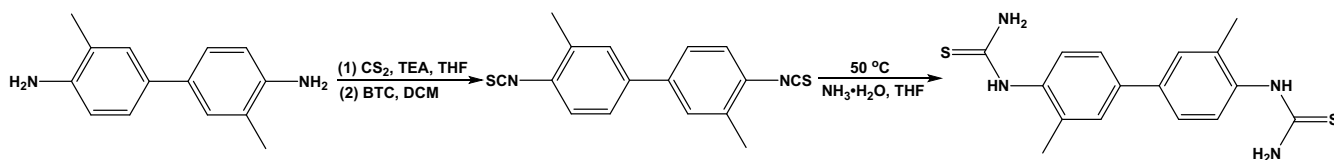
Monomer synthesis:



1,1'-(1,4-phenylene) bis(thiourea) (TU): 1,4-diisothiocyanatobenzene (1 g) was added to a 20 mL ammonium hydroxide solution (28–30%) at room temperature, and a small amount of THF was added to the reaction system. The resulting reaction mixture was stirred at 50 °C for 2 hours. Then the reaction mixture was cooled to room temperature. The product was collected via filtration, washed with water (25 mL), THF (25 mL) and dried in vacuum at 50 °C in 90% yield. ¹H NMR (400 MHz, DMSO) δ 9.64 (s, 2H), 7.33 (s, 8H); ¹³C NMR (100 MHz, DMSO) δ 181.49 (s, 1H), 136.00 (s, 1H), 124.24 (s, 3H); HRMS (ESI-TOF): Calcd for C₈H₁₀N₄S₂H⁺[M+H]⁺ 227.0420, Found 227.0436.



1,1'-(2,5-dimethyl-1,4-phenylene) bis(thiourea) (DMTU): To 50 mL of THF was added 2,5-dimethylbenzene-1,4-diamine (20 mmol, 2.72 g), TEA (100 mmol, 13.9 mL) and CS₂ (100 mmol, 6 mL). The resulting reaction mixture was stirred for 12 hours at 40 °C. Then the yellow solid was collected via filtration and 50 mL of DCM was added, triphosgene (BTC, 40 mmol) in DCM was dropwise added at 0 °C. and the reaction proceeded for 4 hours at reflux temperature. The pure 1,4-diisothiocyanato-2,5-dimethylbenzene compound was obtained by flash chromatography on silica gel with PE as elution solvent in 8% yield. The resulting 1,4-diisothiocyanato-2,5-dimethylbenzene compound (0.5 g) was added to a 15 mL ammonium hydroxide solution (28–30%) at room temperature, and a small amount of THF was added to the reaction system. The resulting reaction mixture was stirred at 50 °C for 2 hours. Then the reaction mixture was cooled to room temperature. The product was collected via filtration, washed with water (20 mL), THF (20 mL) and dried in vacuum at 50 °C in 94% yield. ¹H NMR (600 MHz, DMSO) δ 9.30 (s, 2H), 7.72 (s, 2H), 7.02 (s, 2H), 6.52 (s, 2H), 2.11 (s, 6H); ¹³C NMR (150 MHz, DMSO) δ 181.7, 135.7, 133.6, 130.2, 17.4. HRMS (ESI-TOF): Calcd for C₁₀H₁₄N₄S₂H⁺[M+H]⁺ 255.0738, 255.0766.



1,1'-(3,3'-dimethyl-[1,1'-biphenyl]-4,4'-diyl) bis(thiourea) (DMPTU): To 50 mL of THF was added 3,3'-dimethyl-[1,1'-biphenyl]-4,4'-diamine (20 mmol, 4.24 g), TEA (100 mmol, 13.9 mL) and CS₂ (100 mmol, 6 mL). The resulting reaction mixture was stirred for 12 hours at 40 °C. Then the yellow solid was collected via filtration and 50 mL of DCM was added, triphosgene (BTC, 40 mmol) in DCM was dropwise added at 0 °C. Then, the reaction proceeded for 4 hours at reflux temperature. The pure 4,4'-diisothiocyanato-3,3'-dimethyl-1,1'-biphenyl compound was obtained by flash chromatography on silica gel with PE as elution solvent in 12% yield. The resulting compound (1 g) was added to a 20 mL ammonium hydroxide solution (28–30%) at room temperature, and a small amount of THF was added to the reaction system. The resulting reaction mixture was stirred at 50 °C for 2 hours. Then the reaction mixture was cooled to room temperature. The bithiourea product was collected via filtration, washed with water (30 mL), THF (30 mL) and petroleum ether (20 mL) and dried in vacuum at 50 °C in 92% yield. ¹H NMR (600 MHz, DMSO) δ 9.23 (s, 2H), 7.59 (s, 2H), 7.55 (d, *J* = 1.8 Hz, 2H), 7.47 (dd, *J* = 8.4, 1.8 Hz, 2H), 7.31 (d, *J* = 8.4 Hz, 2H), 7.03 (s, 2H), 2.26 (s, 6H); ¹³C NMR (150 MHz, DMSO) δ 182.1, 138.1, 137.0, 135.1, 129.0, 128.3, 124.8, 18.2. HRMS (ESI-TOF): Calcd for C₁₆H₁₈N₄S₂H⁺[M+H]⁺ 331.1051, 331.1064.

Synthesis of TP-TU-COF: A pyrex tube (10 ml) is charged with 1,3,5-Triformylphloroglucinol (20 mg), 1,1'-(1,4-phenylene) bis(thiourea) (32.2 mg), 0.6 mL NMP, 0.4 mL TCB and 0.1 mL of 6 M aqueous acetic acid. The tube was then flash frozen at 77 K and degassed by three freeze-pump-thaw cycles. The tube was sealed off and then heated at 150 °C for 3 days. The collected powder was washed with dimethylacetamide, tetrahydrofuran and acetone and dried at 100 °C under vacuum for 24 hours to get corresponding dark red powder in 82% isolated yield.

Synthesis of TP-DMTU-COF: A pyrex tube (10 ml) is charged with 1,3,5-Triformylphloroglucinol (20 mg), 1,1'-(2,5-dimethyl-1,4-phenylene) bis(thiourea) (36.2 mg), 0.6 mL NMP, 0.4 mL TCB and 0.1 mL of 6 M aqueous acetic acid. The tube was then flash frozen at 77 K and degassed by three freeze-pump-thaw cycles. The tube was sealed off and then heated at 150 °C for 3 days. The collected powder was washed with dimethylacetamide, tetrahydrofuran and acetone and dried at 100 °C under vacuum for 24 hours to get corresponding red powder in 87% isolated yield.

Synthesis of TP-DMPTU-COF: A pyrex tube (10 ml) is charged with 1,3,5-Triformylphloroglucinol (20 mg), 1,1'-(3,3'-dimethyl-[1,1'-biphenyl]-4,4'-diyl) bis(thiourea) (47.0 mg), 0.6 mL NMP, 0.4 mL TCB and 0.1 mL of 6 M aqueous acetic acid. The tube was then flash frozen at 77 K and degassed by three freeze-pump-thaw cycles. The tube was sealed off and then heated at 150 °C for 3 days. The

collected powder was washed with dimethylacetamide, tetrahydrofuran and acetone and dried at 100 °C under vacuum for 24 hours to get corresponding dark red powder in 89% isolated yield.

The procedure of Knoevenagel reaction about aldehydes and malononitrile: A reaction ground tube (10 ml) is charged with COF catalyst (2 mol%), aldehydes (0.3 mmol), malononitrile (0.3 mmol), toluene (2 mL) and H₂O (0.4 mL). After being stirred at 60 °C for 10 h, the solvent was removed and the pure product was obtained by flash chromatography on silica gel.

Section B. Supporting Figures

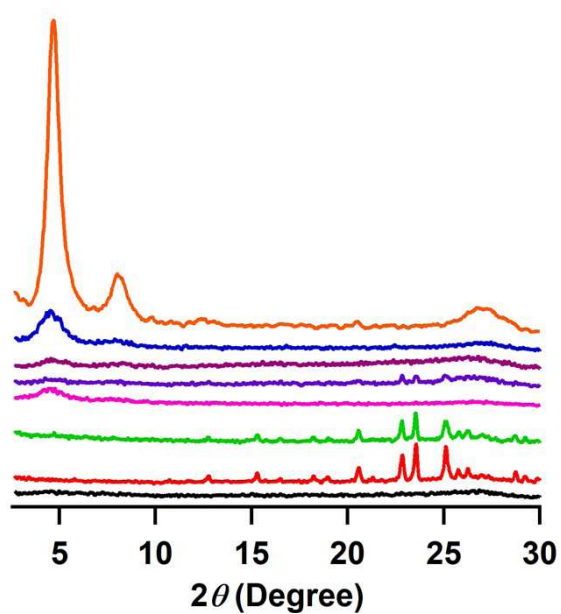


Figure S1. XRD profiles of the TP-TU-COF synthesized under different conditions. black: NMP/TCB/6 M AcOH (4:6:1 by vol., 90 °C); red: NMP/TCB/6 M AcOH (2:8:1 by vol., 90 °C); green: n-BuOH/TCB/6 M AcOH (5:5:1 by vol., 90 °C); pink: NMP/TCB/6 M AcOH (4:6:1 by vol., 120 °C); violet: NMP/TCB/6 M AcOH (2:8:1 by vol., 120 °C); purple: NMP/TCB/6 M AcOH (6:4:1 by vol., 180 °C); blue: NMP/TCB/6 M AcOH (6:4:1 by vol., 120 °C); orange: NMP/TCB/6 M AcOH (6:4:1 by vol., 150 °C).

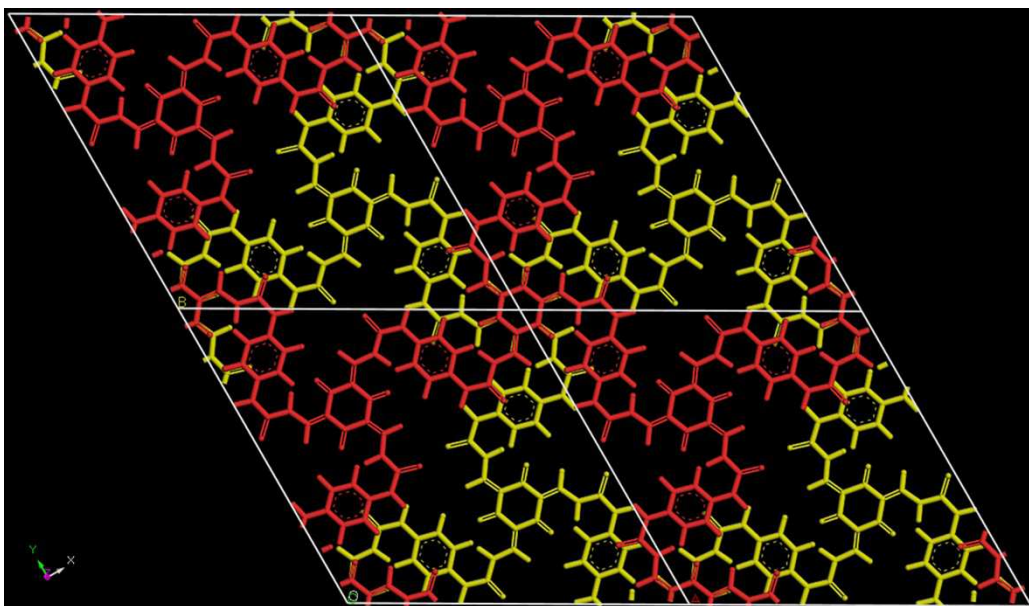


Figure S2. Reproduced AB stacking crystal structure of TP-TU-COF.

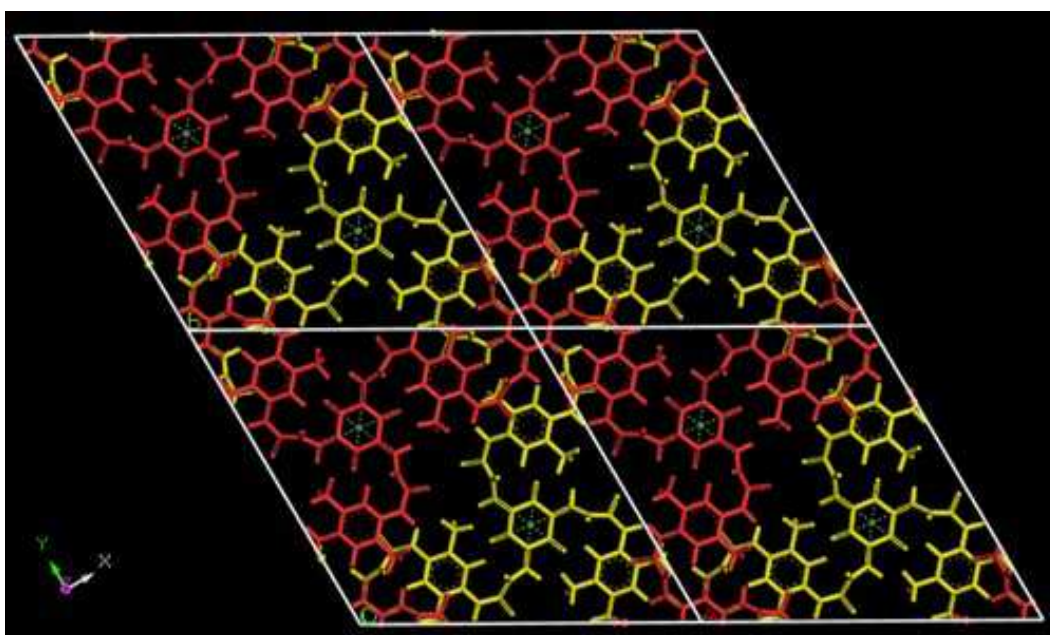


Figure S3. Reproduced AB stacking crystal structure of TP-DMTU-COF.

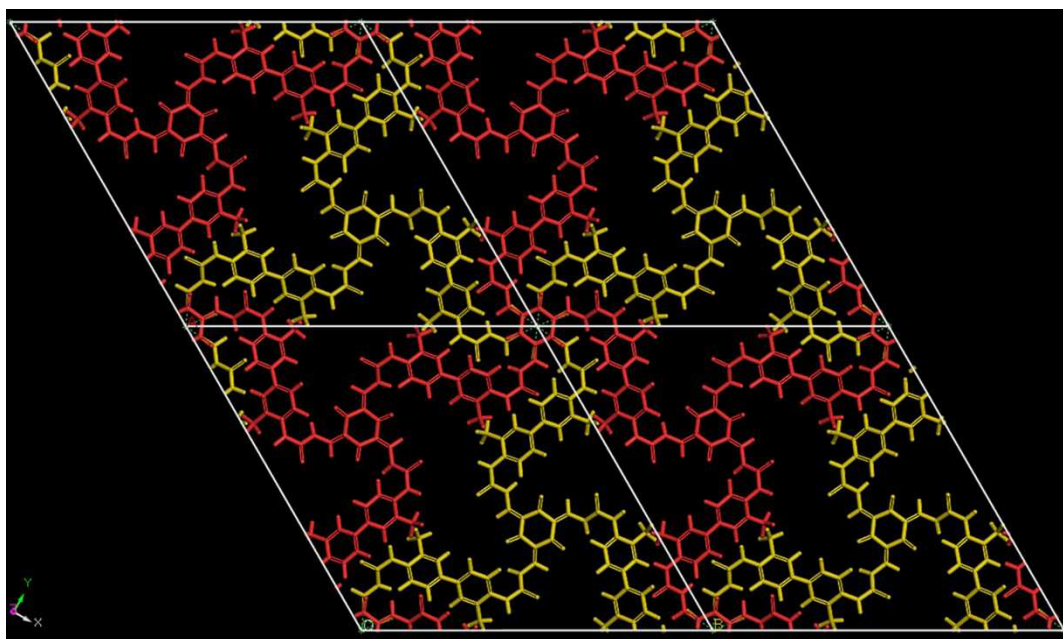


Figure S4. Reproduced AB stacking crystal structure of TP-DMPTU-COF.

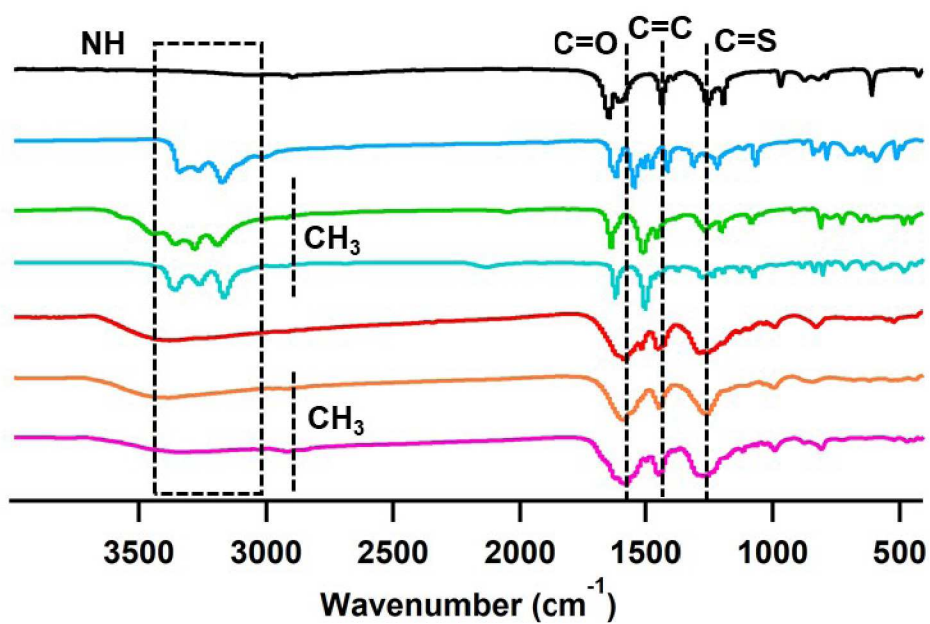


Figure S5. FT-IR spectra of (red) TP-TU-COF, (orange) TP-DMTU-COF, and (pink) TP-DMPTU-COF and corresponding monomers (black) TP, (blue) TU, (green) DMTU, and (dark green).

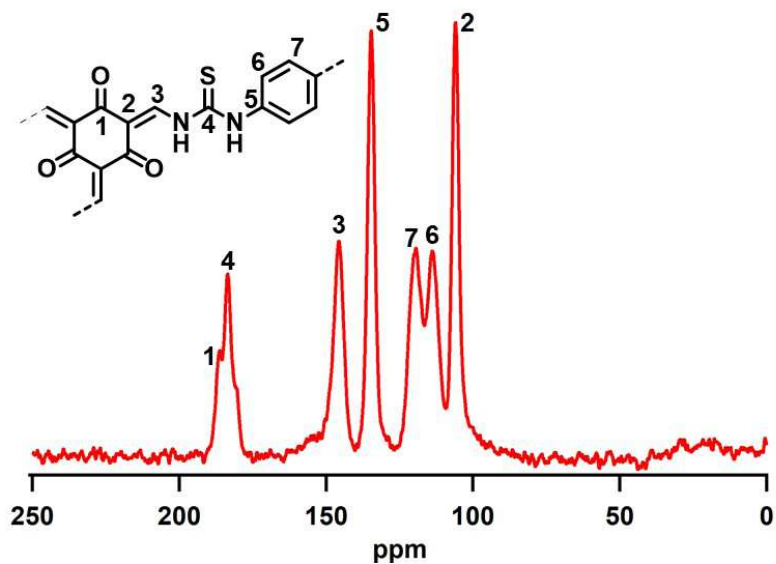


Figure S6. ^{13}C CP/MAS solid-state NMR spectra of TP-TU-COF.

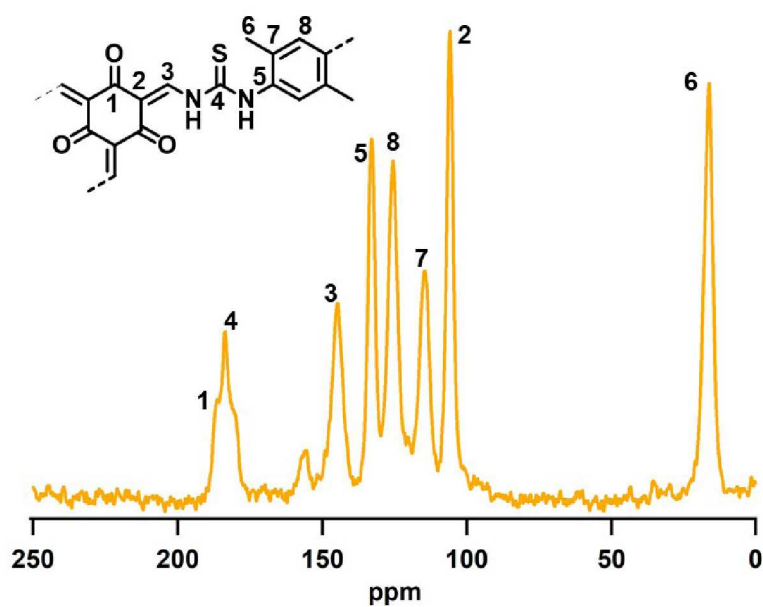


Figure S7. ^{13}C CP/MAS solid-state NMR spectra of TP-DMTU-COF.

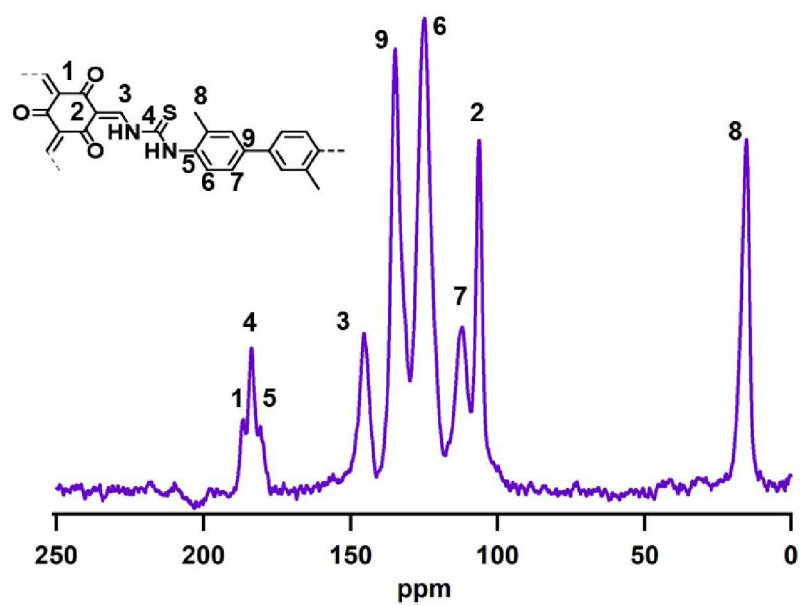


Figure S8. ^{13}C CP/MAS solid-state NMR spectra of TP-DMPTU-COF.

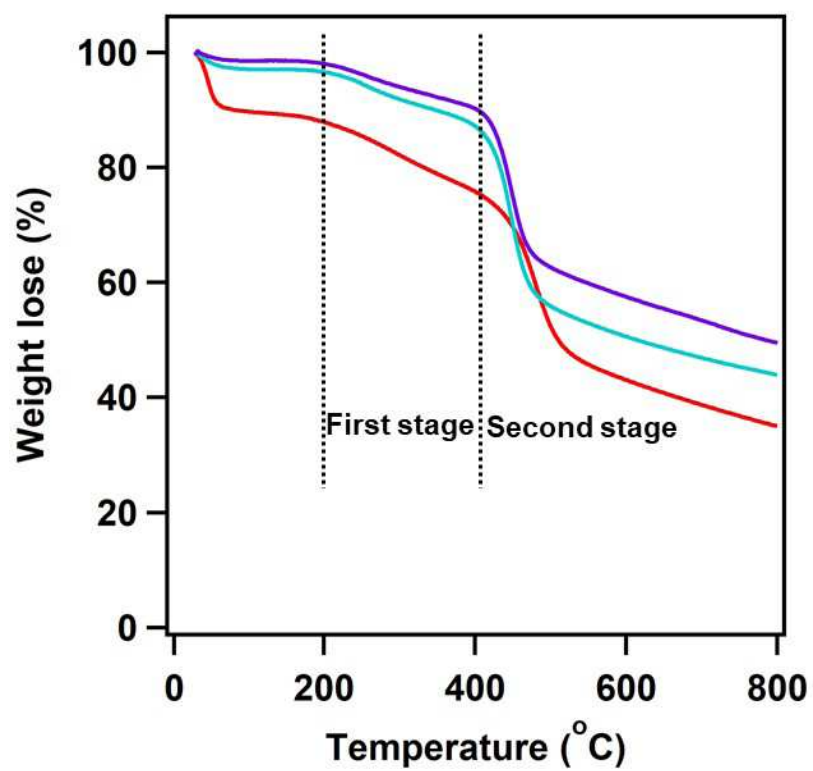


Figure S9. Thermogravimetric curves of (red) TP-TU-COF, (green) TP-DMTU-COF, and (purple) TP-DMPTU-COF.

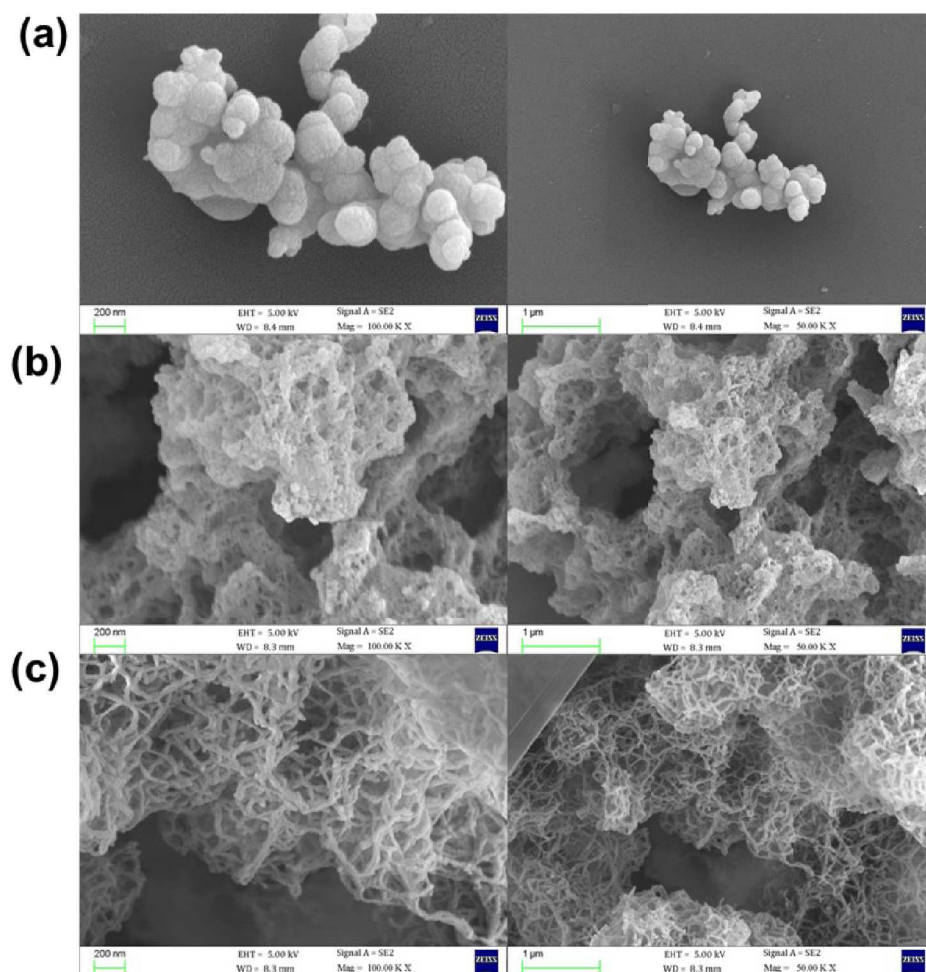


Figure S10. SEM images of (a) TP-TU-COF, (b) TP-DMTU-COF, and (c) TP-DMPTU-COF.

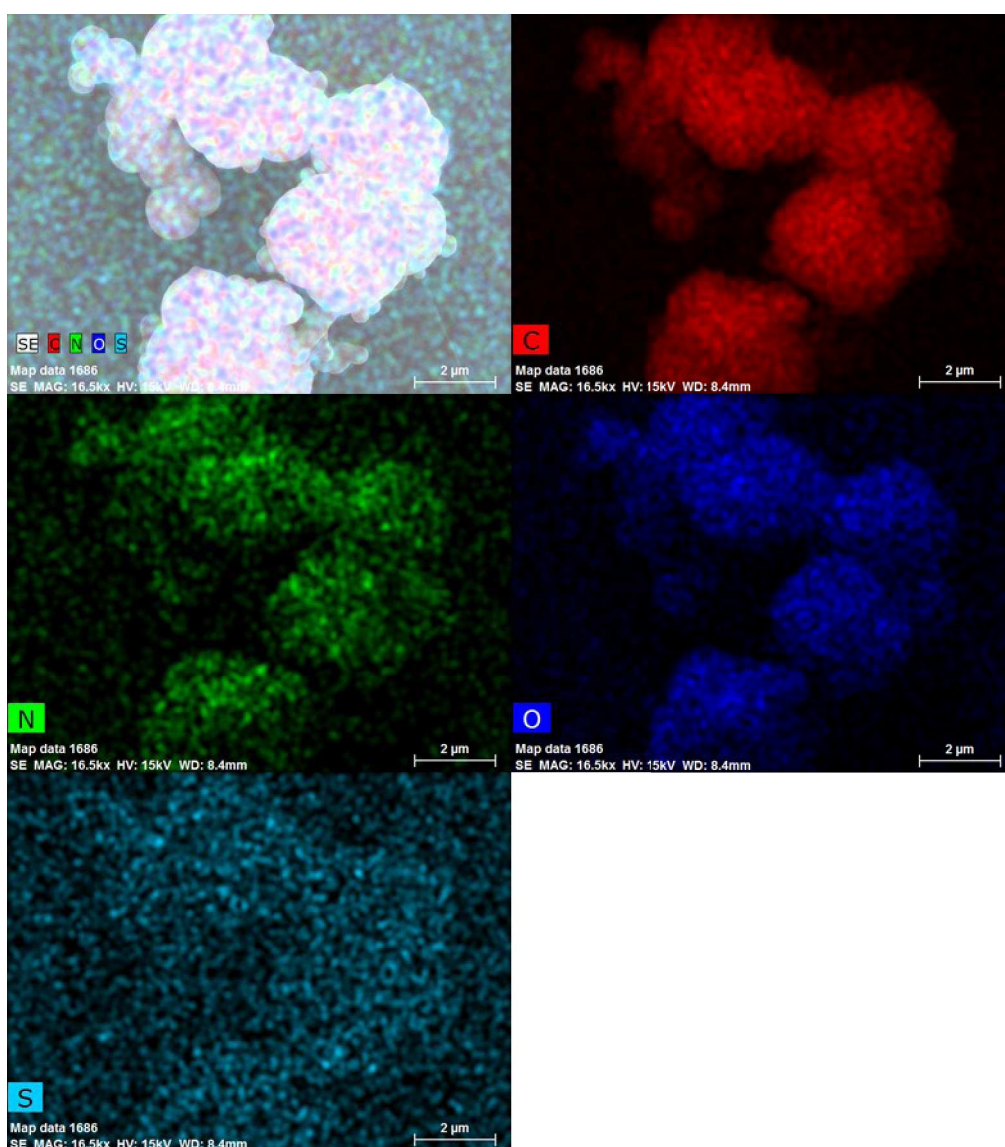


Figure S11. Elemental distribution mapping of TP-TU-COF.

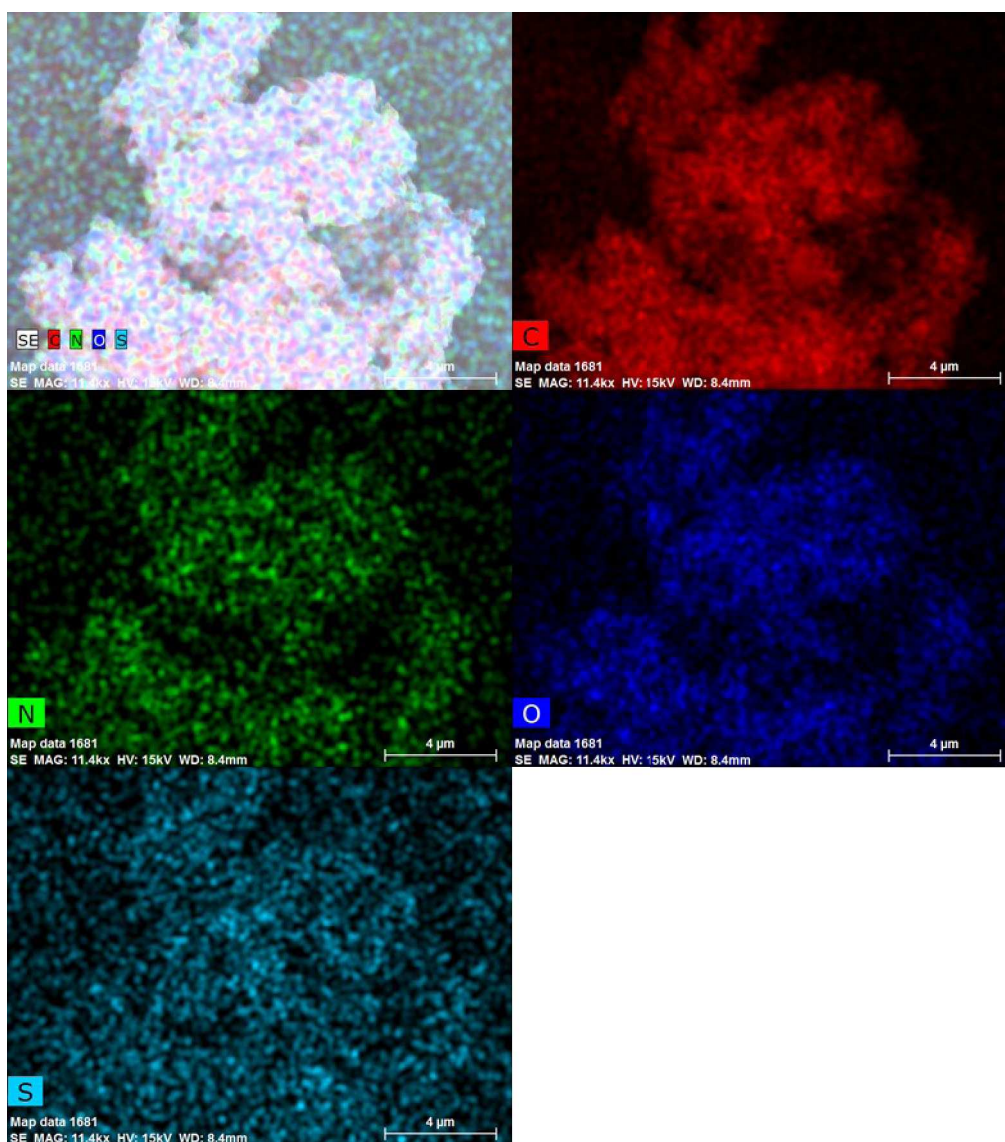


Figure S12. Elemental distribution mapping of TP-DMTU-COF.

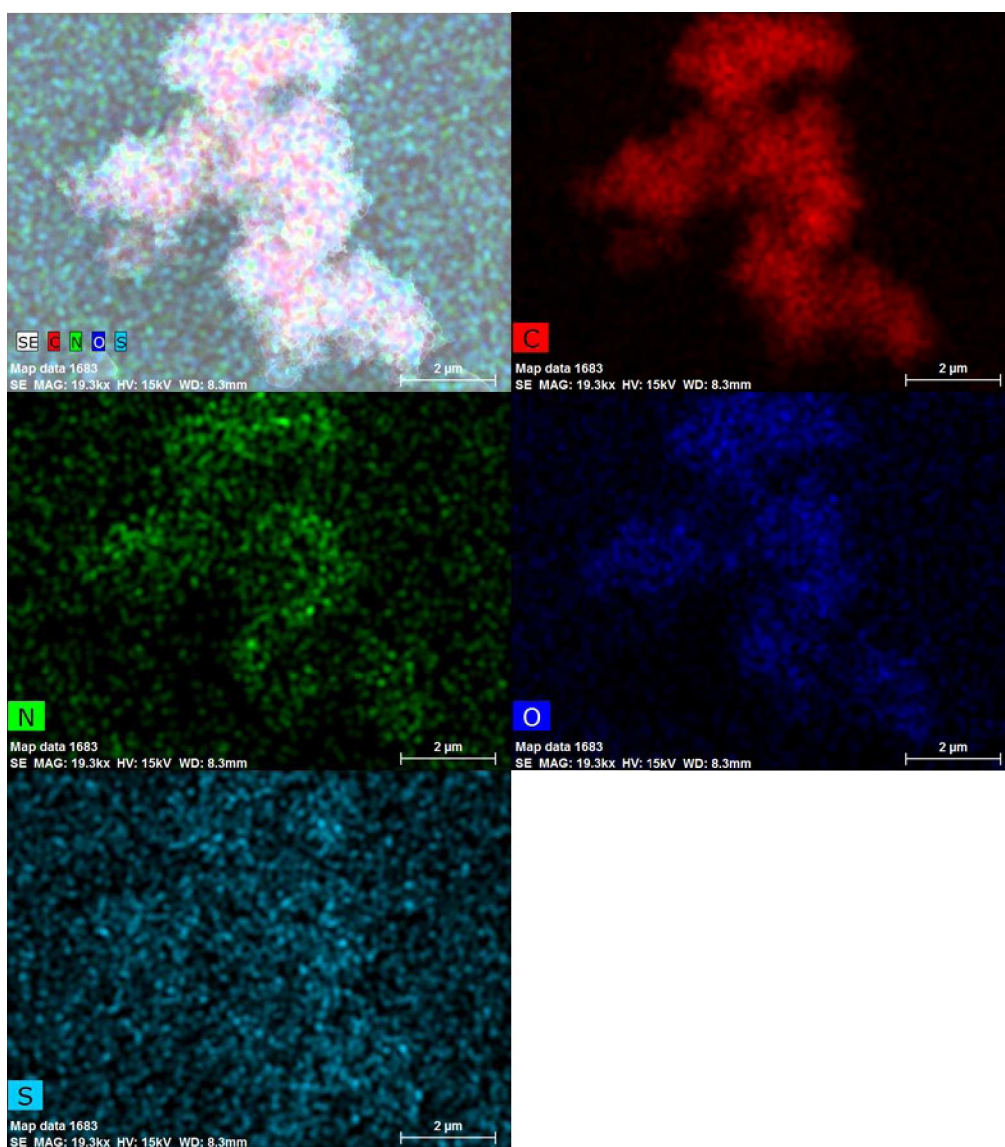


Figure S13. Elemental distribution mapping of TP-DMPTU-COF.

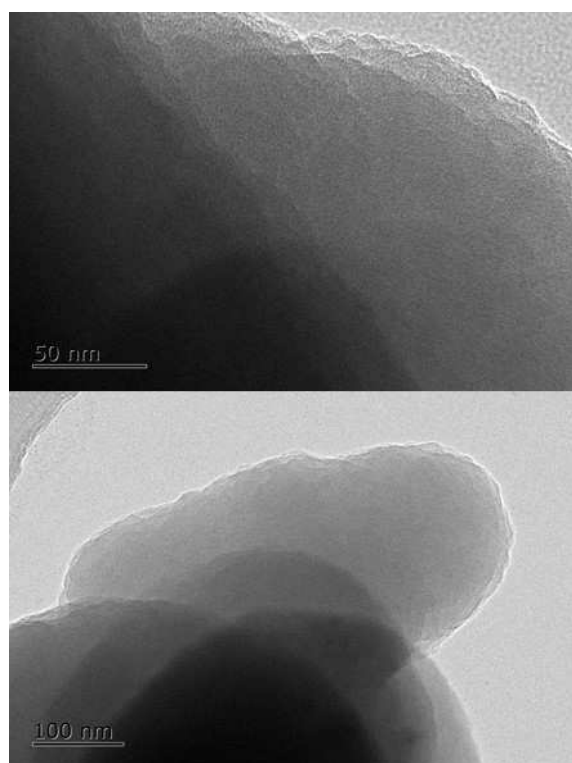


Figure S14. TEM images of TP-TU-COF.

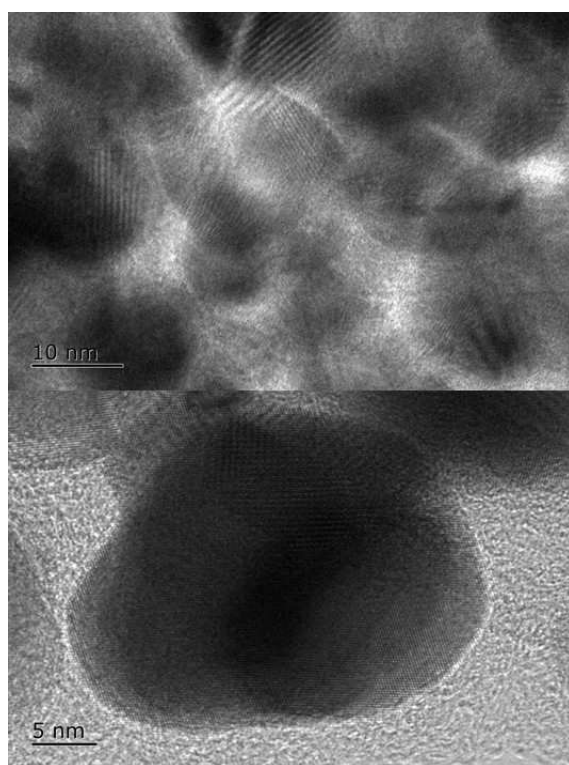


Figure S15. TEM images of TP-DMTU-COF.

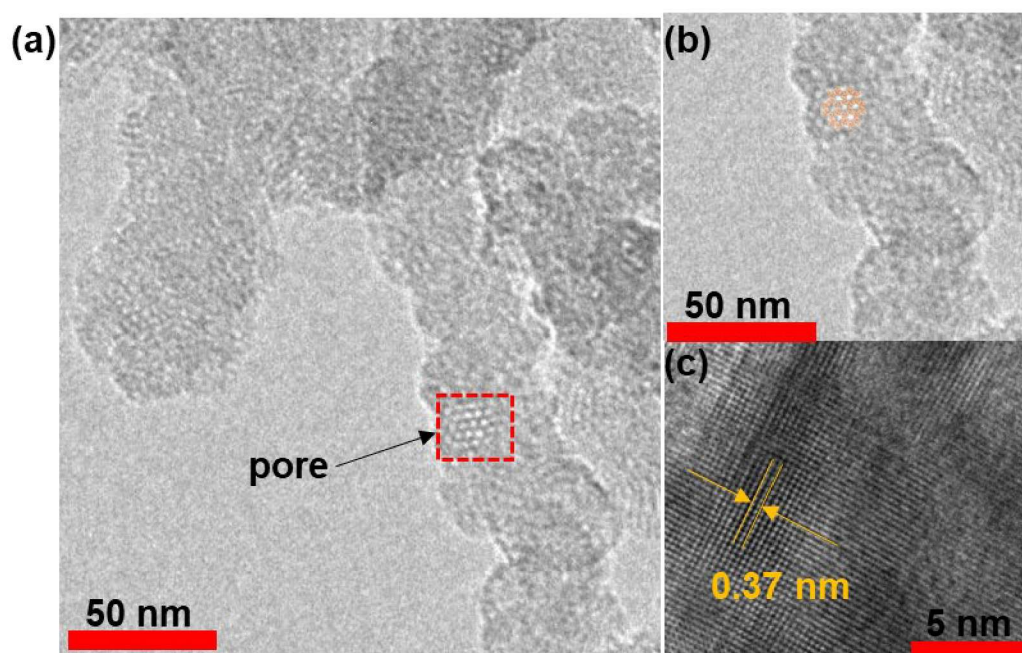


Figure S16. TEM images of TP-DMPTU-COF: (a, b) hexagonal pores, TEM image of TP-DMPTU-COF showing hexagonal pores viewing from [001] direction, and (c) layer distance.

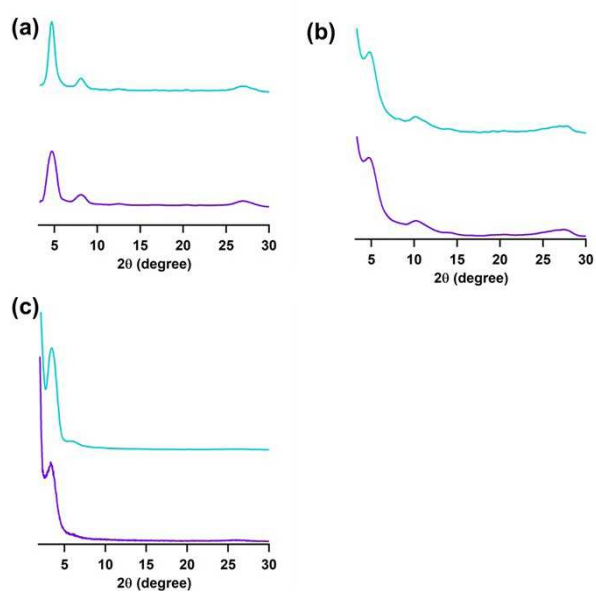


Figure S17. Chemical stability: PXRD profiles of (a) TP-TU-COF, (b) TP-DMTU-COF, and (c) TP-DMPTU-COF after treatment in HCl (1M, blue) and NaOH (1M, purple).

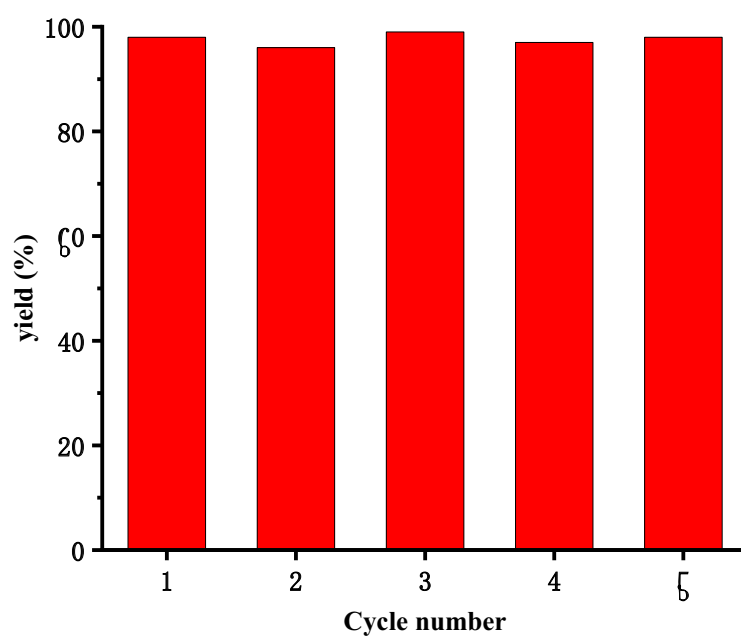


Figure S18. Catalytic activity performance of TP-DMPTU-COF for catalyzing compound 1a for five cycles.

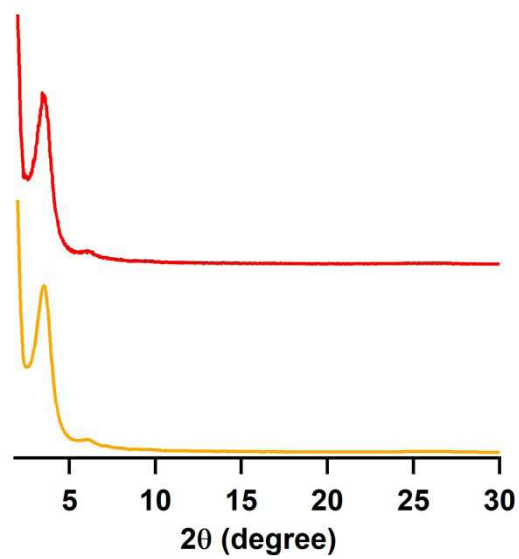
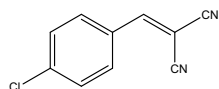
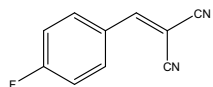


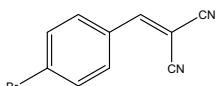
Figure S19. PXRD patterns of TP-DMPTU-COF before (red) and after (yellow) catalytic recycle performance.



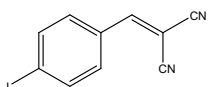
2-(4-chlorobenzylidene)malononitrile(2a): White solid; 97% yield; ^1H NMR (600 MHz, DMSO) δ 8.54 (s, 1H), 8.02-7.90 (m, 2H), 7.77-7.66 (m, 2H); ^{13}C NMR (150 MHz, DMSO) δ 160.6, 139.5, 132.6, 130.6, 130.2, 114.6, 113.5, 82.8.



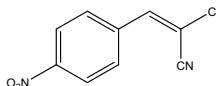
2-(4-fluorobenzylidene)malononitrile(2b): White solid; 92% yield; ^1H NMR (600 MHz, CDCl_3) δ 7.97–7.94 (m, 2H), 7.74 (s, 1H), 7.32–7.16 (m, 2H); ^{13}C NMR (150 MHz, CDCl_3) δ 166.1 (d, J = 259.5 Hz), 158.3, 133.4 (d, J = 10.5 Hz), 127.3, 117.2 (d, J = 22.5 Hz), 113.5, 112.5, 82.4.



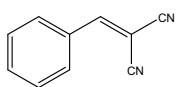
2-(4-bromobenzylidene)malononitrile(2c): White solid; 95% yield; ^1H NMR (600 MHz, CDCl_3) δ 7.77 (d, J = 8.4 Hz, 2H), 7.72 (s, 1H), 7.68 (d, J = 8.4 Hz, 2H); ^{13}C NMR (150 MHz, CDCl_3) δ 158.4, 133.1, 131.8, 129.9, 129.6, 113.4, 112.3, 83.5.



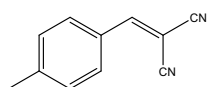
2-(4-iodobenzylidene)malononitrile(2d): White solid; 97% yield; ^1H NMR (600 MHz, CDCl_3) δ 7.91 (d, J = 8.4 Hz, 2H), 7.70 (s, 1H), 7.61 (d, J = 8.4 Hz, 2H); ^{13}C NMR (150 MHz, CDCl_3) δ 158.7, 139.0, 131.5, 130.1, 113.4, 112.3, 102.8, 83.5.



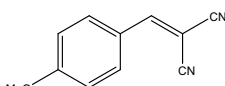
2-(4-nitrobenzylidene)malononitrile(2e): White solid; 89% yield; ^1H NMR (600 MHz, CDCl_3) δ 8.39 (d, J = 9.0 Hz, 2H), 8.08 (d, J = 9.0 Hz, 2H), 7.89 (s, 1H); ^{13}C NMR (150 MHz, CDCl_3) δ 156.8, 150.3, 135.8, 131.3, 124.6, 112.6, 111.6, 87.5.



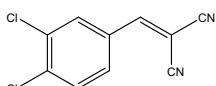
benzylidenemalononitrile(2f): White solid; 99% yield; ^1H NMR (600 MHz, CDCl_3) δ 7.89 (d, J = 7.8 Hz, 2H), 7.76 (s, 1H), 7.62 (t, J = 7.5 Hz, 1H), 7.52 (t, J = 7.8 Hz, 2H); ^{13}C NMR (150 MHz, CDCl_3) δ 159.9, 134.6, 130.9, 130.7, 129.6, 113.7, 112.5, 82.8.



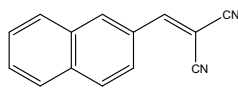
2-(4-methylbenzylidene)malononitrile(2g): White solid; 98% yield; ^1H NMR (600 MHz, CDCl_3) δ 7.81 (d, J = 7.8 Hz, 2H), 7.71 (s, 1H), 7.33 (d, J = 7.8 Hz, 2H), 2.45 (s, 3H); ^{13}C NMR (150 MHz, CDCl_3) δ 159.7, 146.4, 130.9, 130.4, 128.4, 114.0, 112.8, 81.2, 22.0.



2-(4-methoxybenzylidene)malononitrile(2h): White solid; 95% yield; ^1H NMR (600 MHz, CDCl_3) δ 7.93–7.90 (m, 2H), 7.65 (s, 1H), 7.03–7.00 (m, 2H), 3.92 (s, 3H); ^{13}C NMR (150 MHz, CDCl_3) δ 164.8, 158.9, 133.4, 124.0, 115.1, 114.4, 113.3, 99.9, 78.5, 55.8.

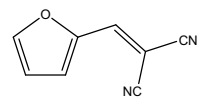


2-(3,4-dichlorobenzylidene)malononitrile(2i): White solid; 97% yield; ^1H NMR (600 MHz, CDCl_3) δ 7.92 (d, J = 1.8 Hz, 1H), 7.80 (dd, J = 8.4, 1.8 Hz, 1H), 7.68 (s, 1H), 7.62 (d, J = 8.4 Hz, 1H); ^{13}C NMR (151 MHz, CDCl_3) δ 156.93 (s, 3H), 139.19 (s, 1H), 134.40 (s, 1H), 132.29 (s, 4H), 131.75 (s, 3H), 130.43 (s, 1H), 128.95 (s, 3H), 113.0, 111.9, 84.8.



2-(naphthalen-2-ylmethylene)malononitrile(2j): Yellow green solid; 85% yield; ^1H NMR (600 MHz, CDCl_3) δ 8.27 (s, 1H), 8.06 (dd, J = 8.4, 1.8 Hz, 1H), 7.96-7.93 (m, 2H), 7.90 (d, J = 8.4 Hz, 2H), 7.88 (s, 1H), 7.68 (t, J = 7.5 Hz, 1H), 7.61 (t, J = 7.5 Hz, 1H); ^{13}C NMR (150 MHz, CDCl_3) δ 159.7, 135.9, 134.5, 132.6, 130.0, 129.7, 128.5, 128.0, 127.7, 124.2, 114.0, 112.8, 82.2.

2-((2,3-dihydrobenzo[b][1,4]dioxin-6-yl)methylene)malononitrile(2k): Yellow solid; 96% yield; ^1H NMR (600 MHz, CDCl_3) δ 7.57 (s, 1H), 7.50 (d, $J = 1.8$ Hz, 1H), 7.42 (dd, $J = 9.0$, 2.4 Hz, 1H), 6.96 (d, $J = 9.0$ Hz, 1H), 4.36-4.35 (m, 2H), 4.30-4.28 (m, 2H); ^{13}C NMR (150 MHz, CDCl_3) δ 158.8, 149.7, 144.0, 125.9, 124.6, 119.6, 118.4, 114.3, 113.1, 79.2, 64.9, 64.0.



2-(furan-2-ylmethylene) malononitrile(2l): Yellow solid; 99% yield; ^1H NMR (600 MHz, CDCl_3) δ 7.82 (d, $J = 1.6$ Hz, 1H), 7.53 (s, 1H), 7.37 (d, $J = 3.6$ Hz, 1H), 6.73 (dd, $J = 3.6$, 1.8 Hz, 1H); ^{13}C NMR (150 MHz, CDCl_3) δ 149.6, 148.1, 143.1, 123.5, 114.4, 113.8, 112.6.

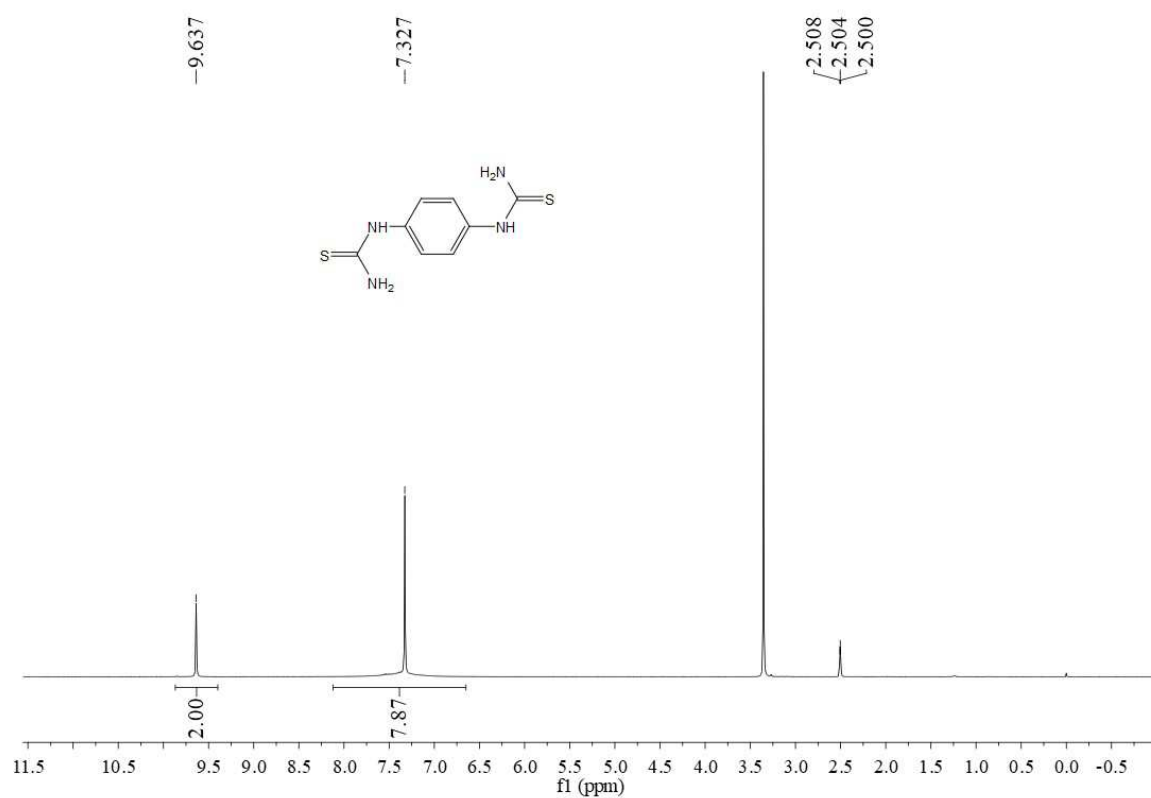


Figure S18. ¹H-NMR spectrum of TU.

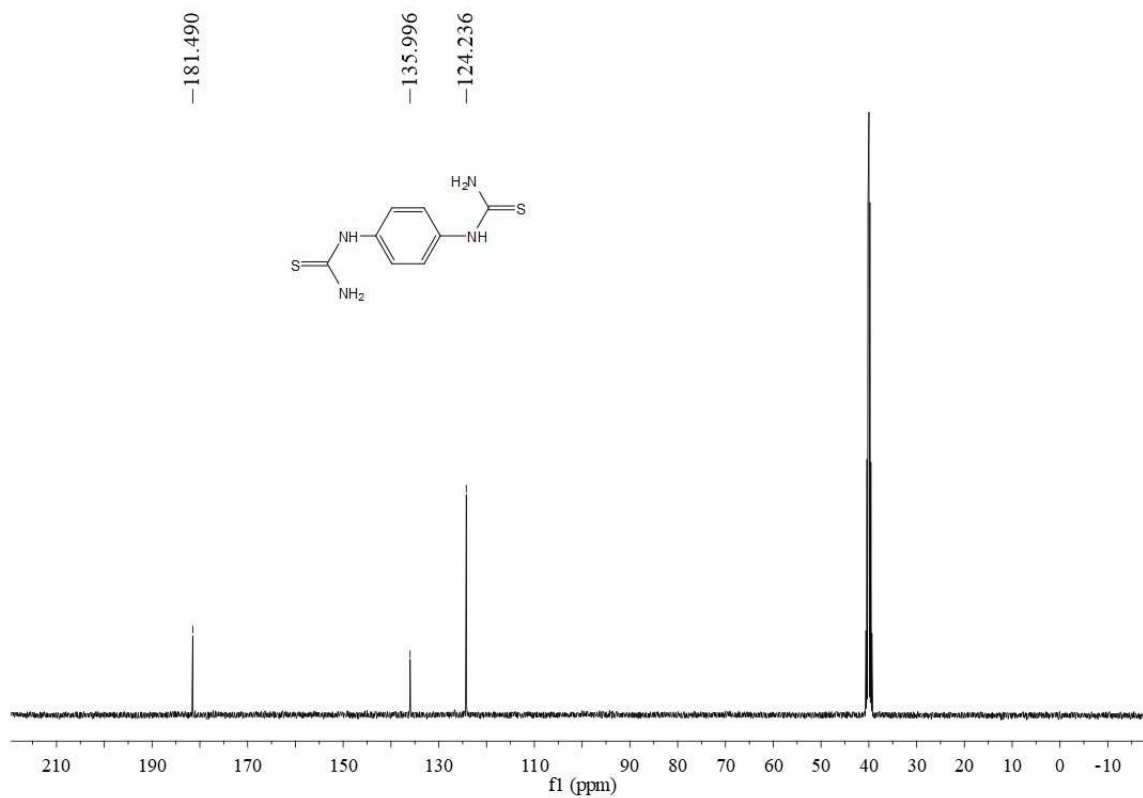


Figure S19. ¹³C-NMR spectrum of TU.

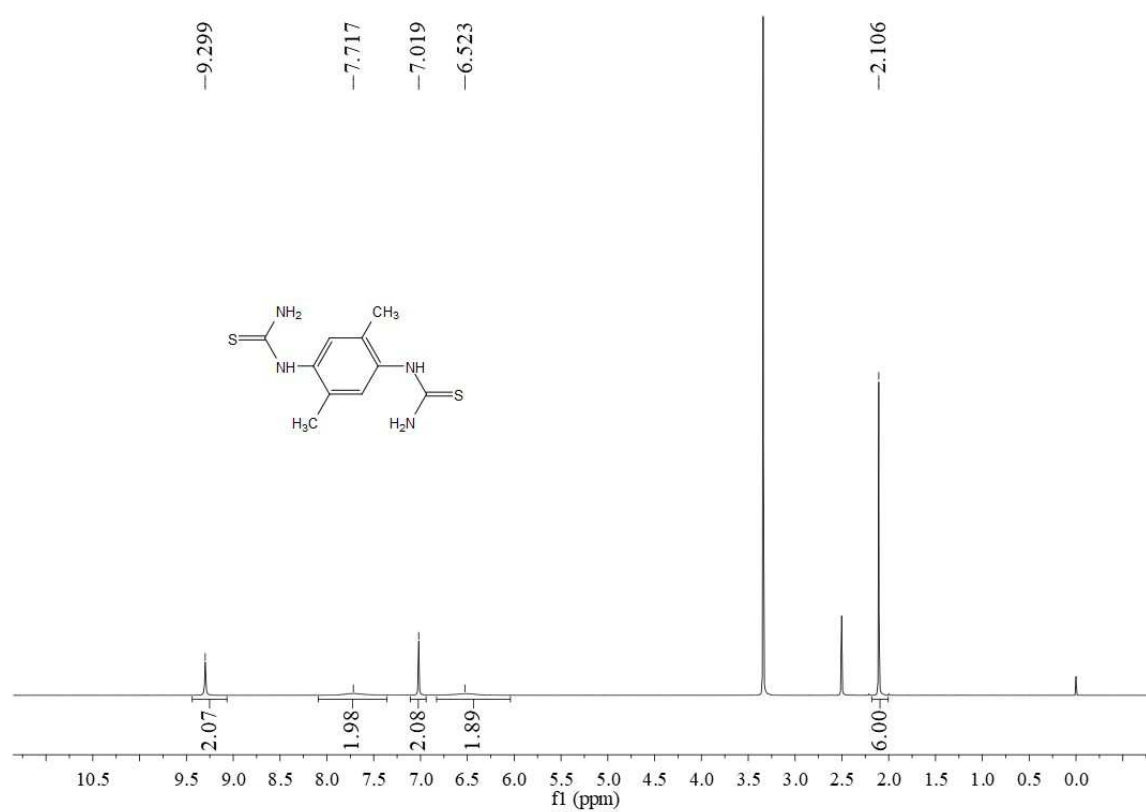


Figure S20. ¹H-NMR spectrum of DMTU.

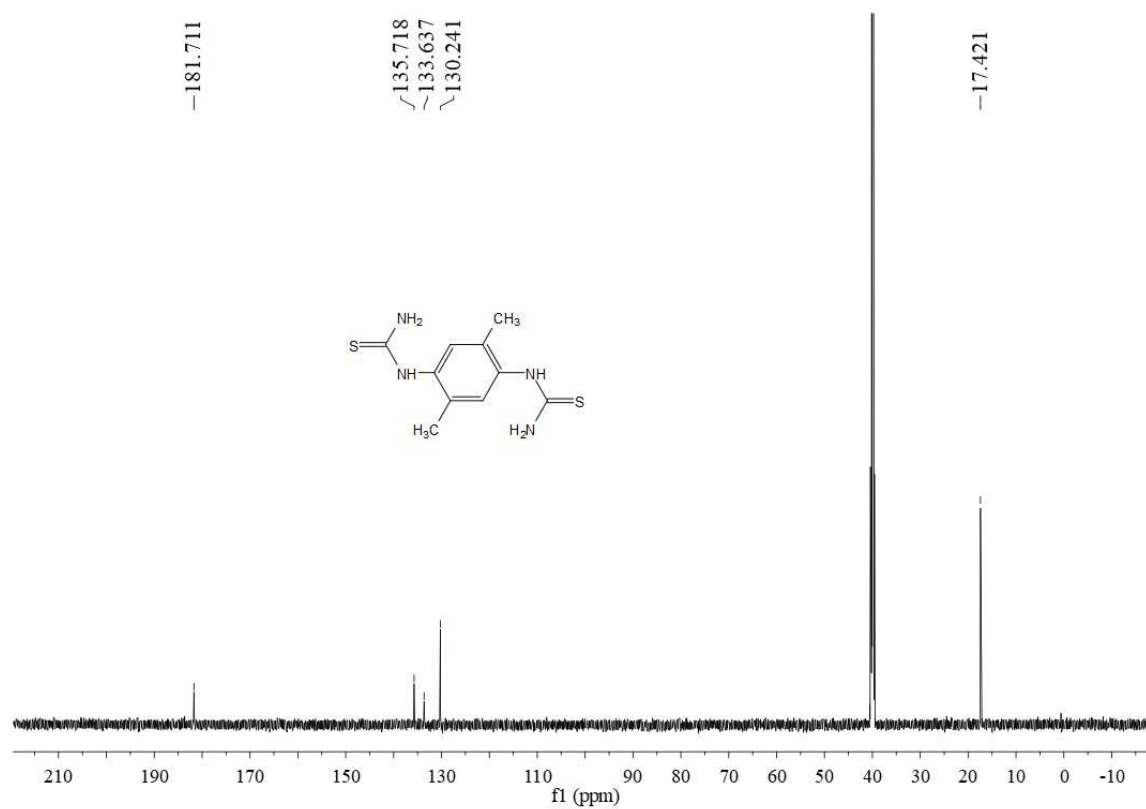


Figure S21. ¹³C-NMR spectrum of DMTU.

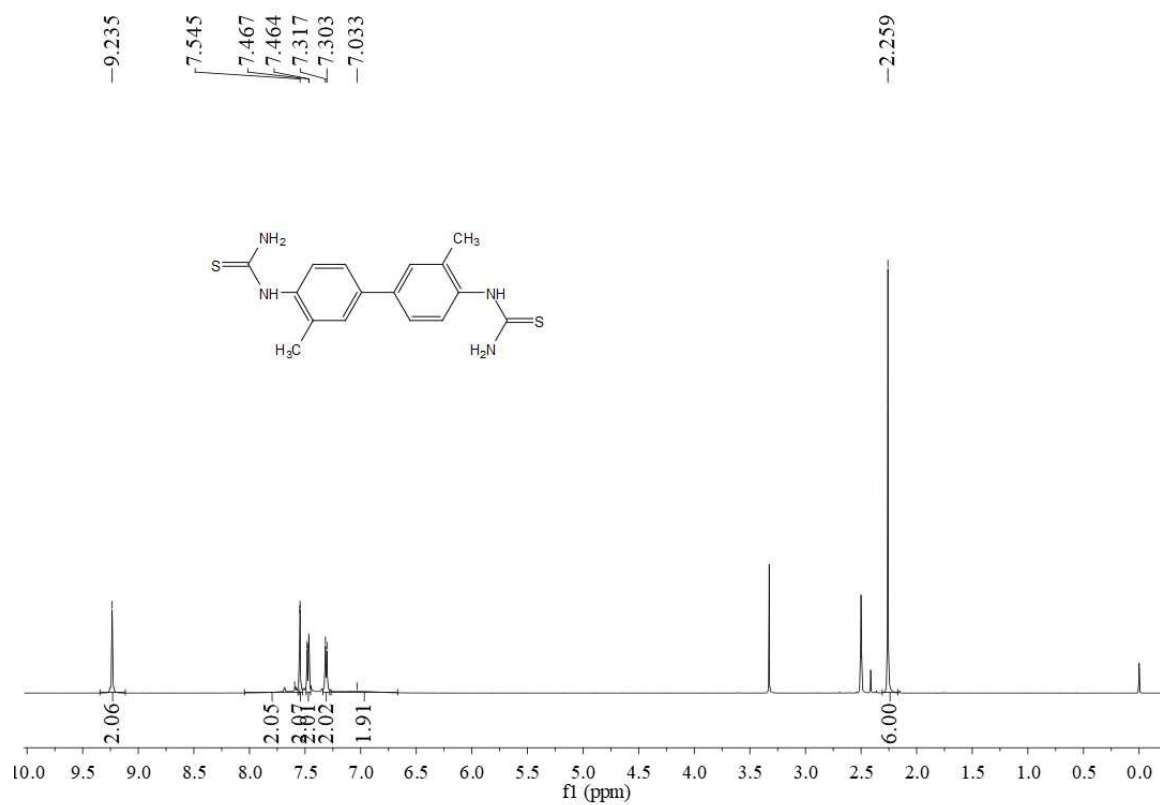


Figure S22. ¹H-NMR spectrum of DMPTU.

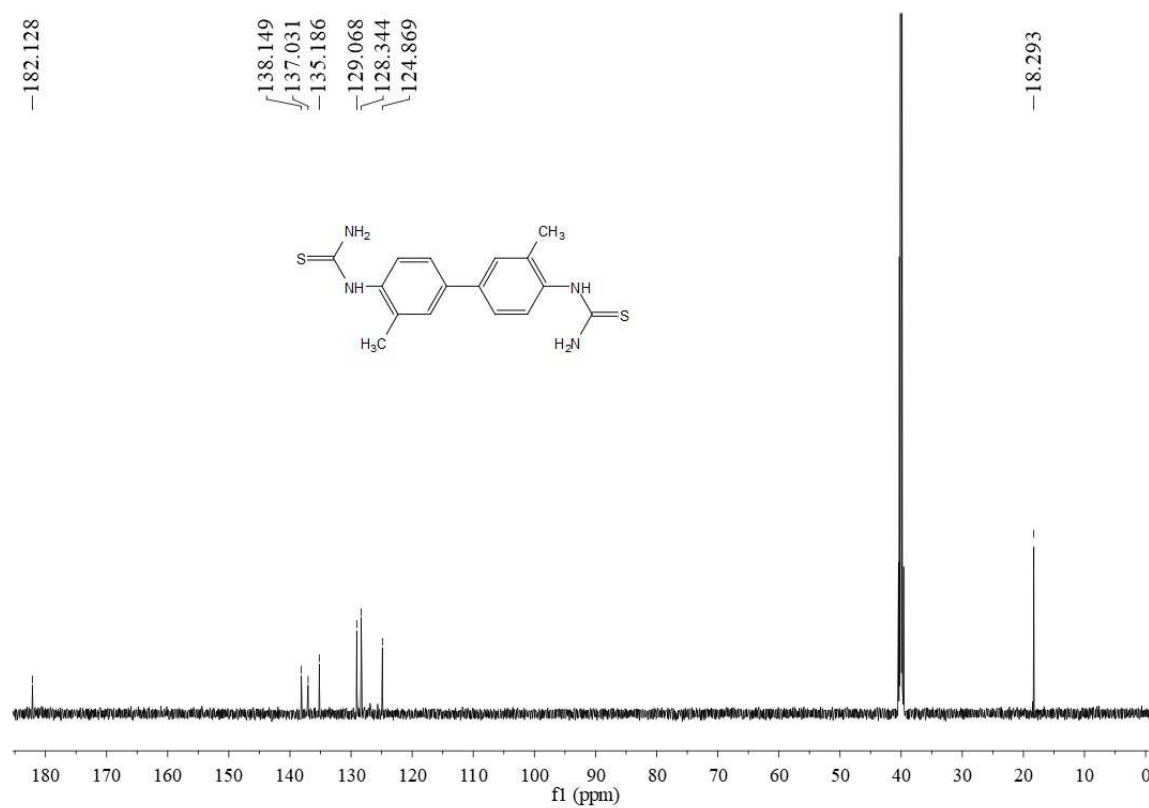


Figure S23. ¹³C-NMR spectrum of DMPTU.

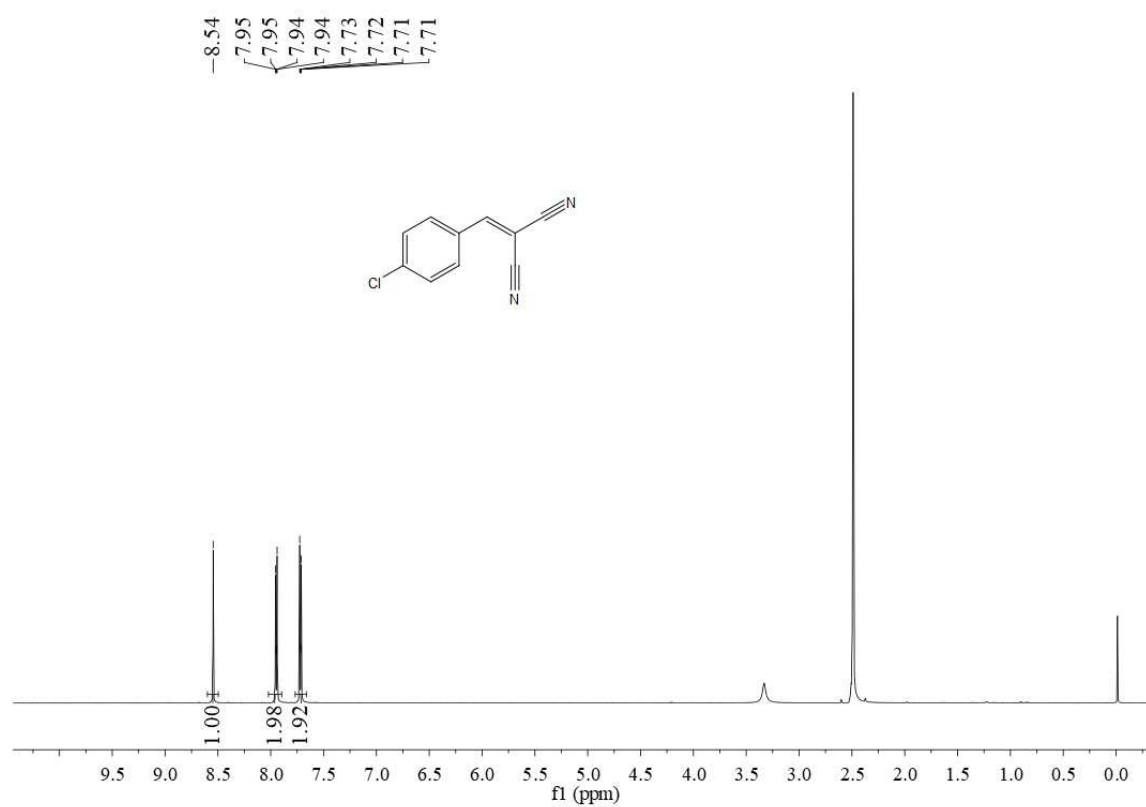


Figure S24. ¹H-NMR spectrum of 2a.

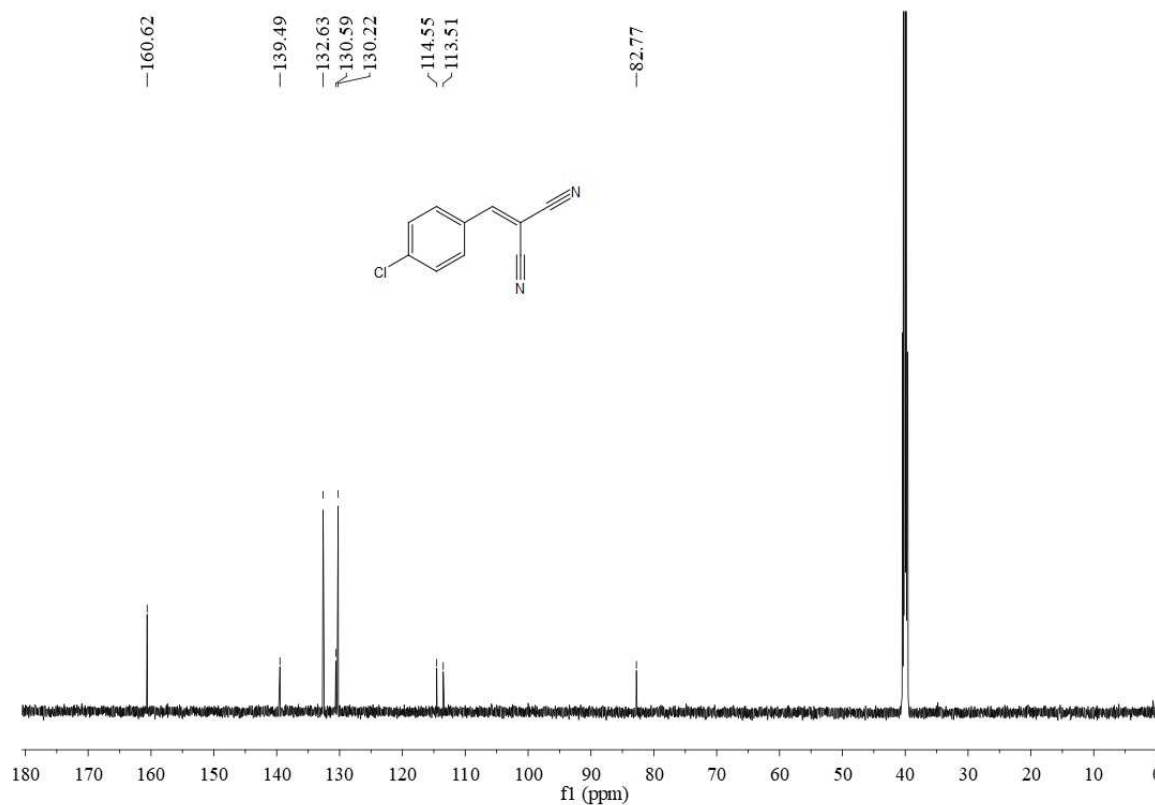


Figure S25. ¹³C-NMR spectrum of 2a.

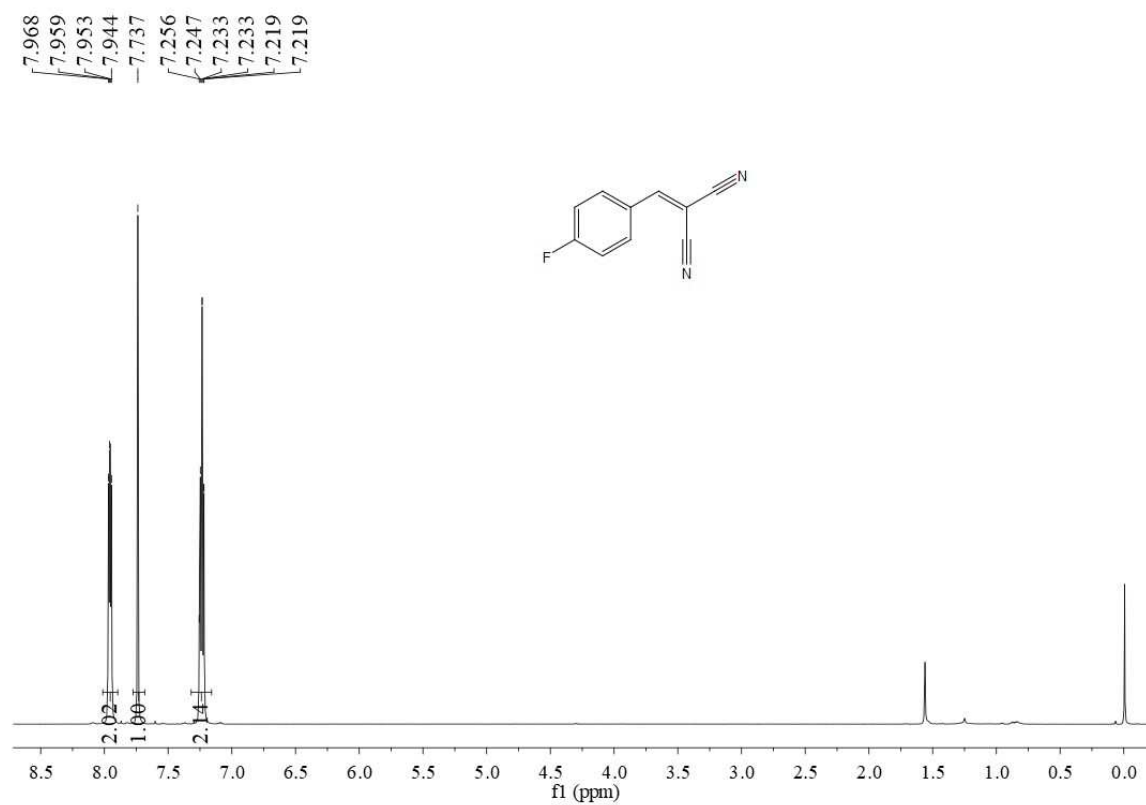


Figure S26. ¹H-NMR spectrum of **2b**.

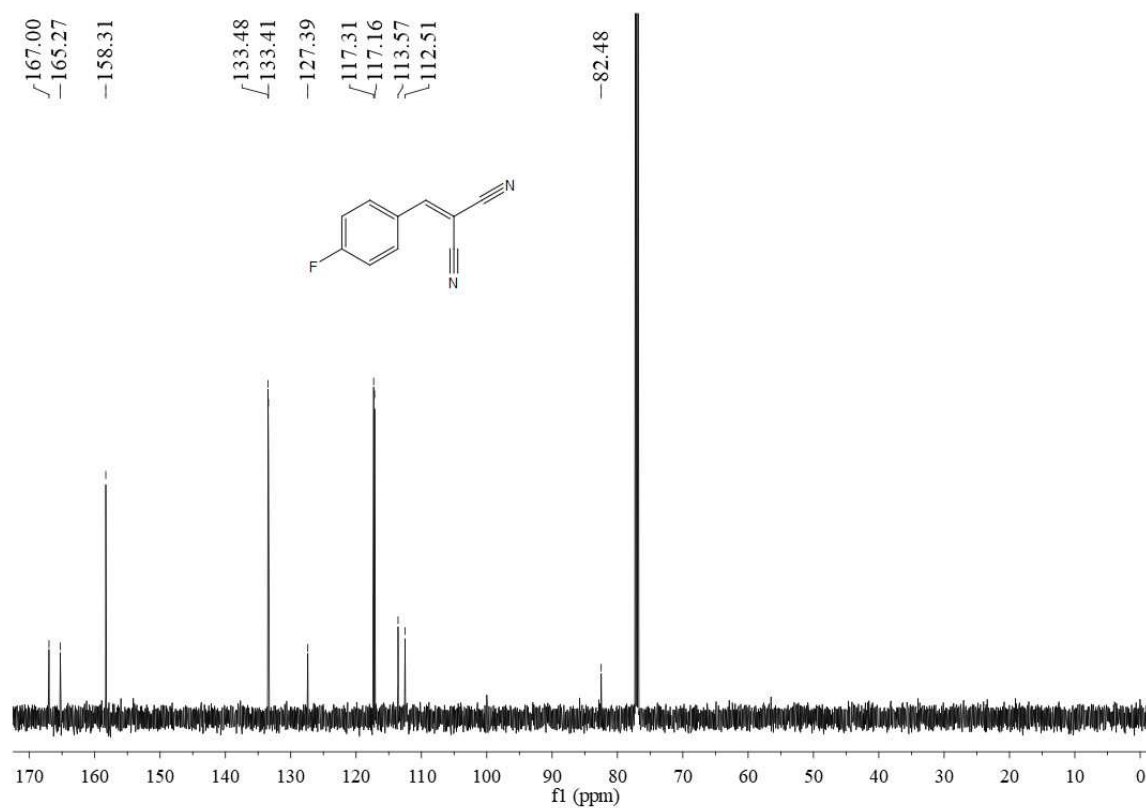


Figure S27. ¹³C-NMR spectrum of **2b**.

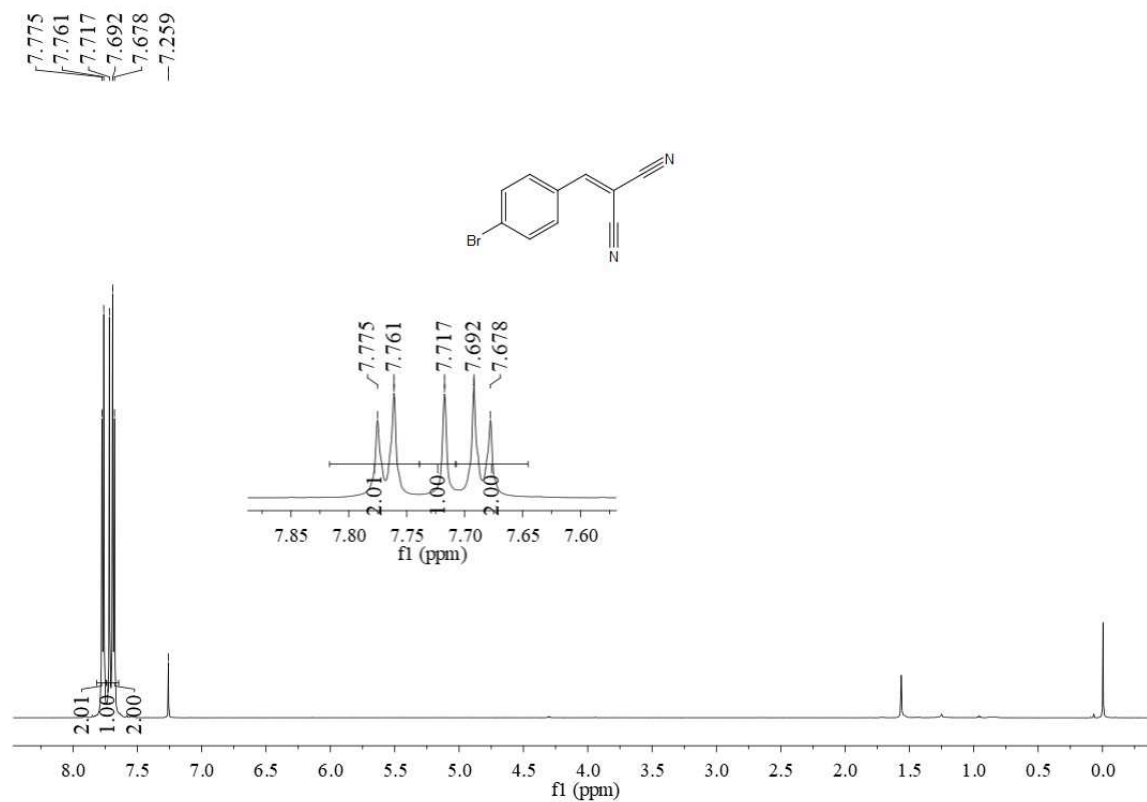


Figure S28. ¹H-NMR spectrum of 2c.

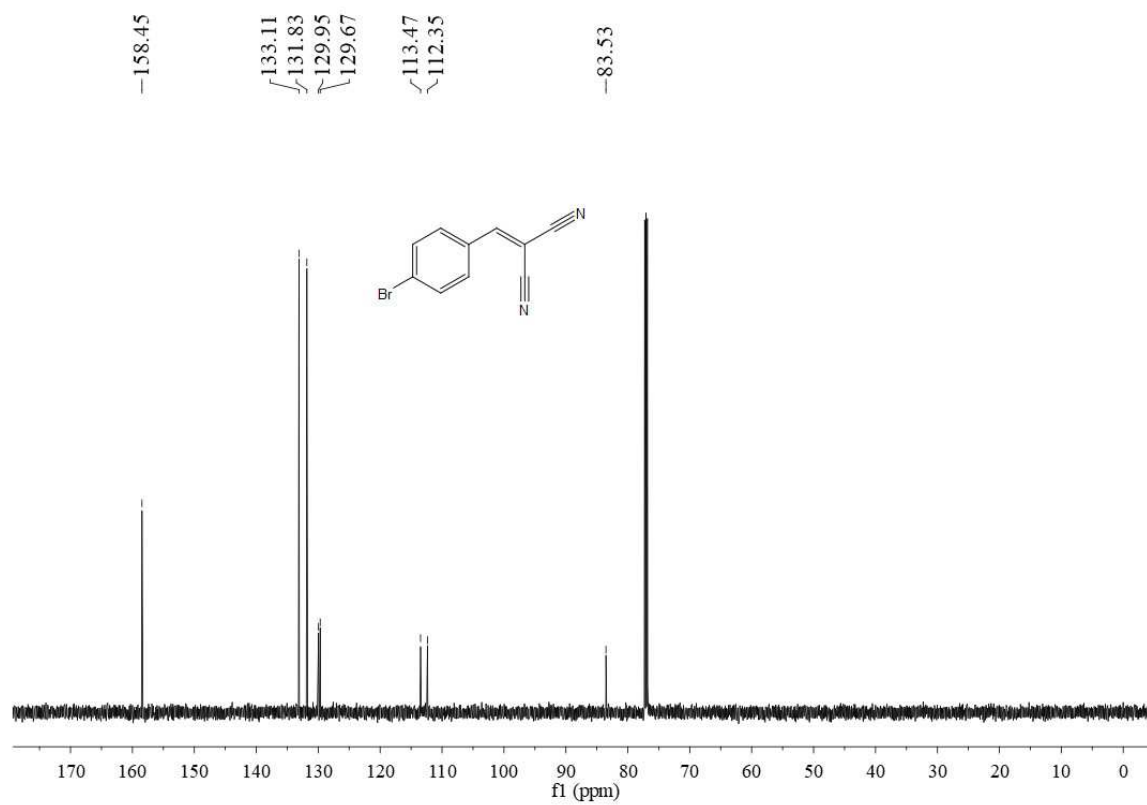


Figure S29. ¹³C-NMR spectrum of 2c.

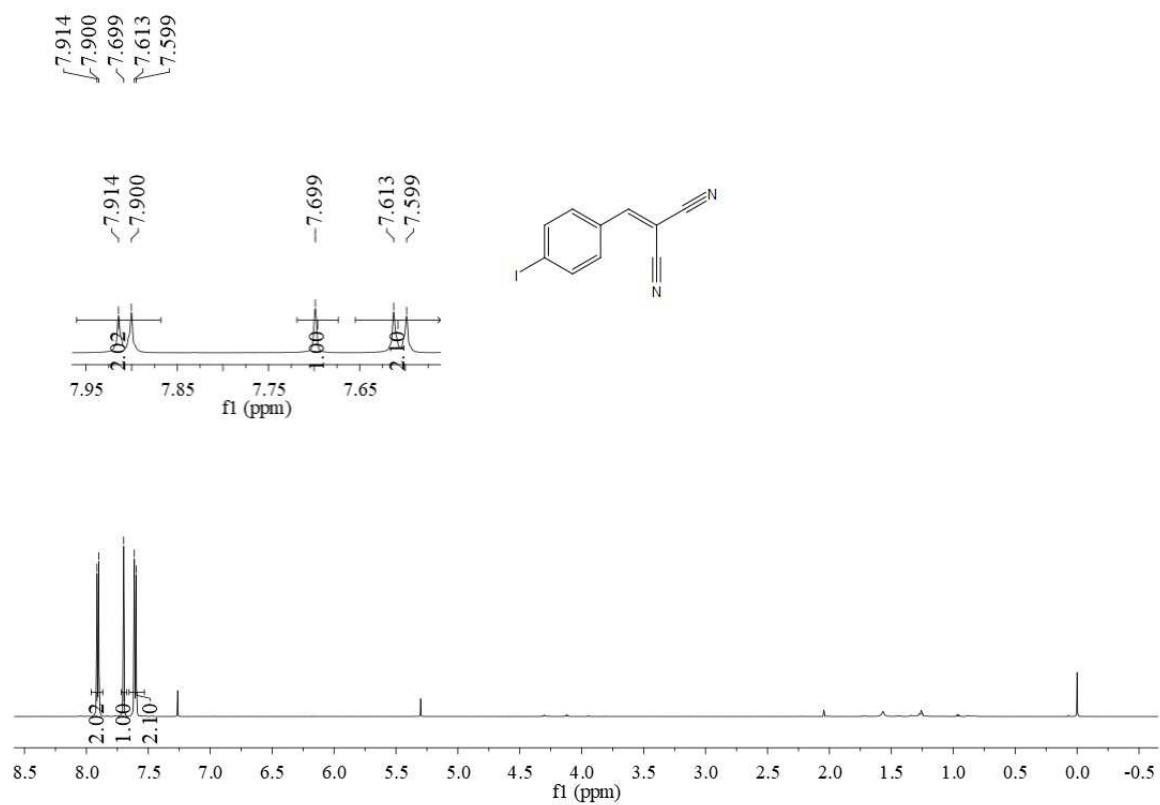


Figure S30. ¹H-NMR spectrum of 2d.

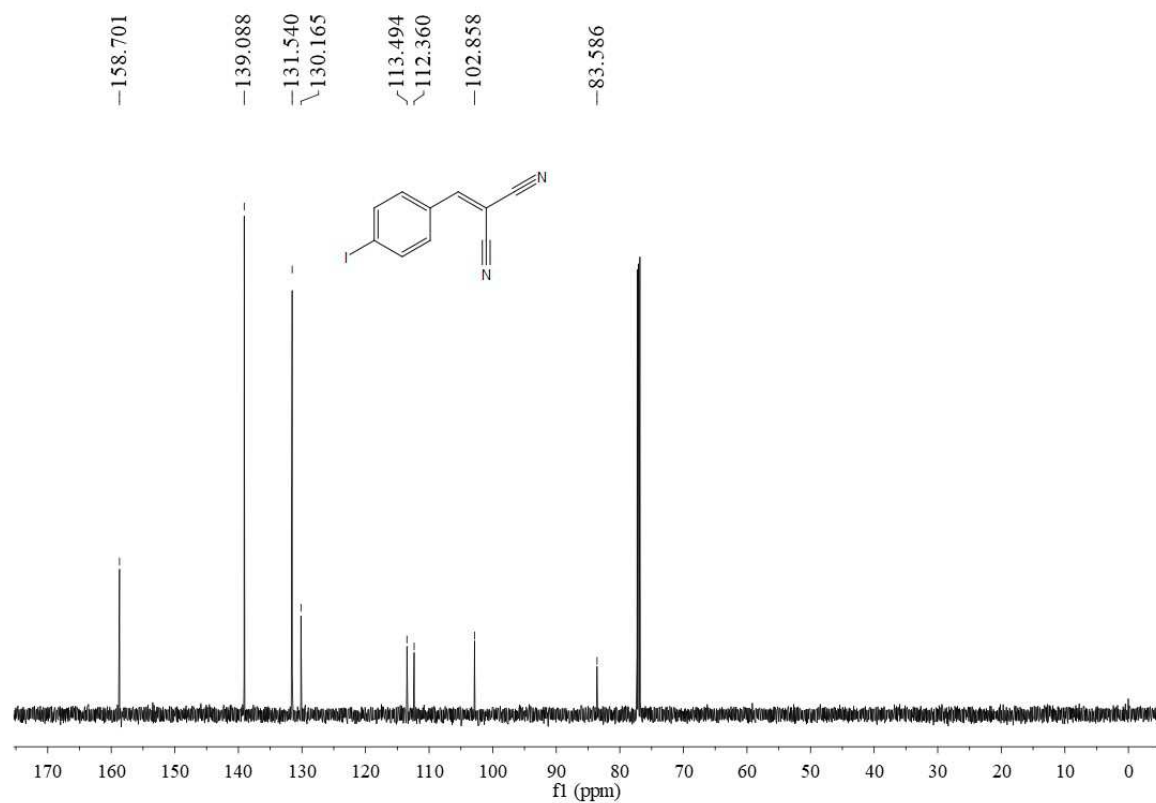


Figure S31. ¹³C-NMR spectrum of 2d.

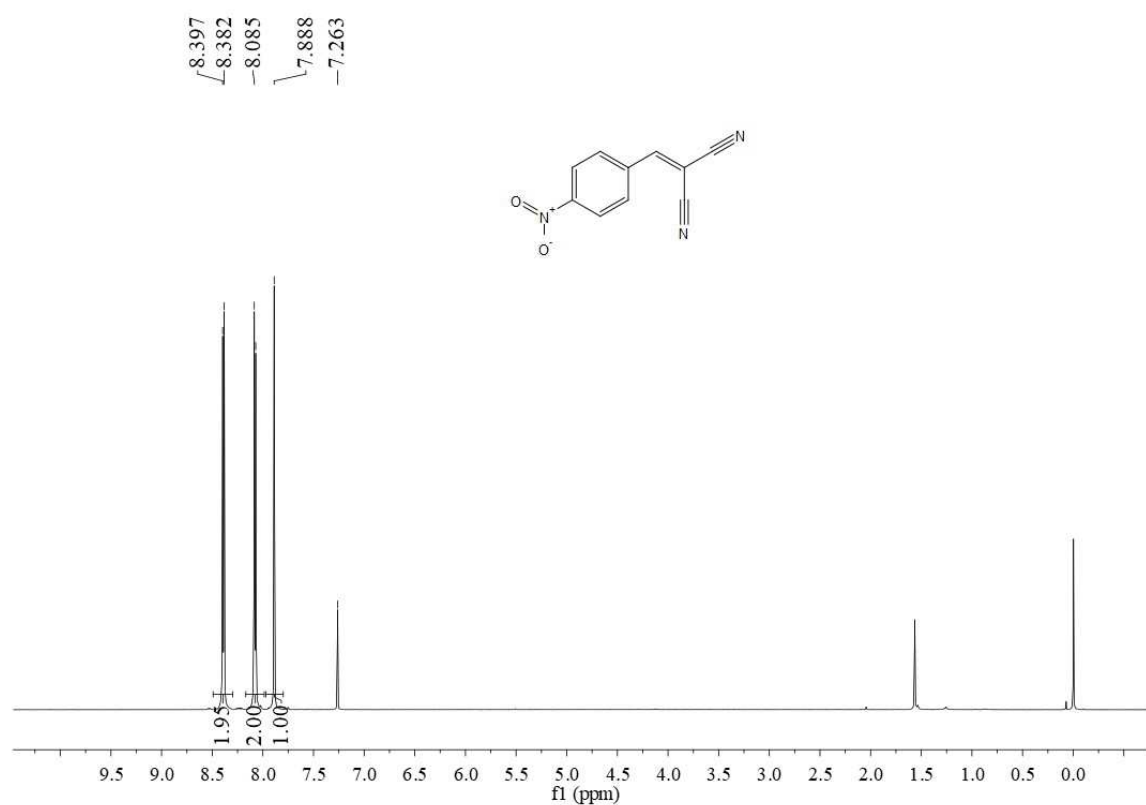


Figure S32. ¹H-NMR spectrum of 2e.

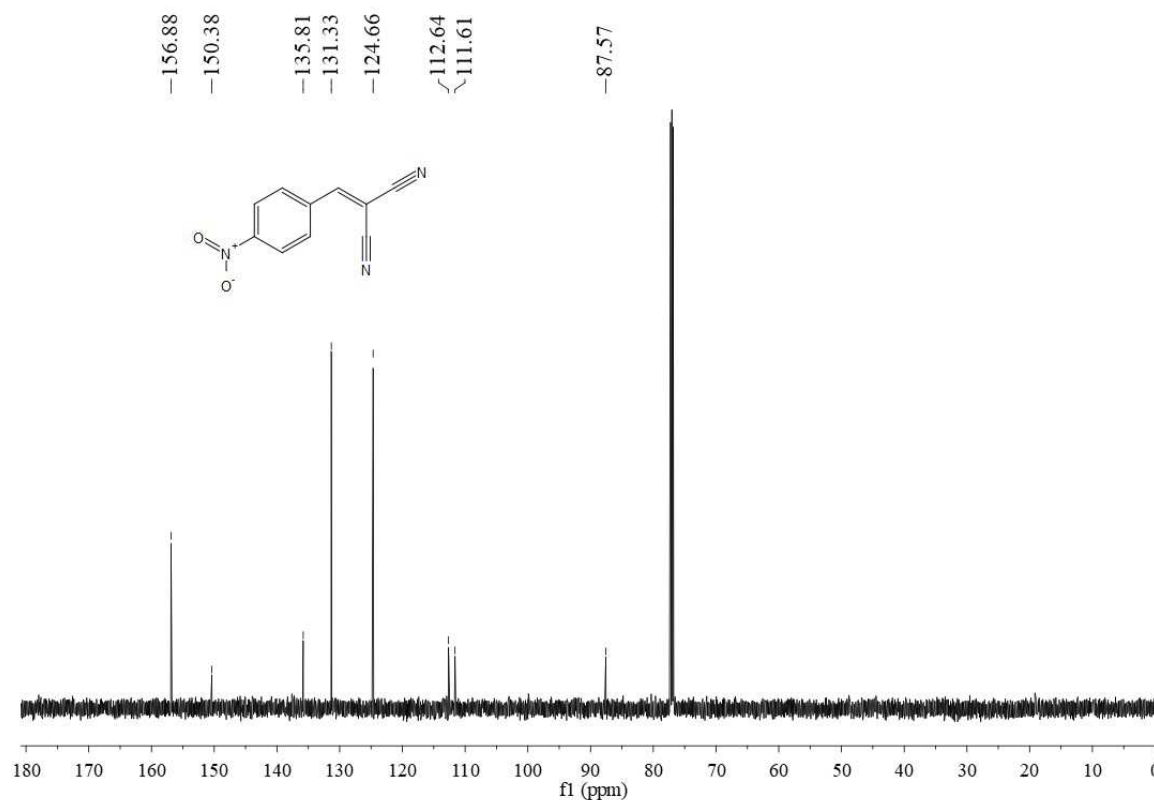


Figure S33. ¹³C-NMR spectrum of 2e.

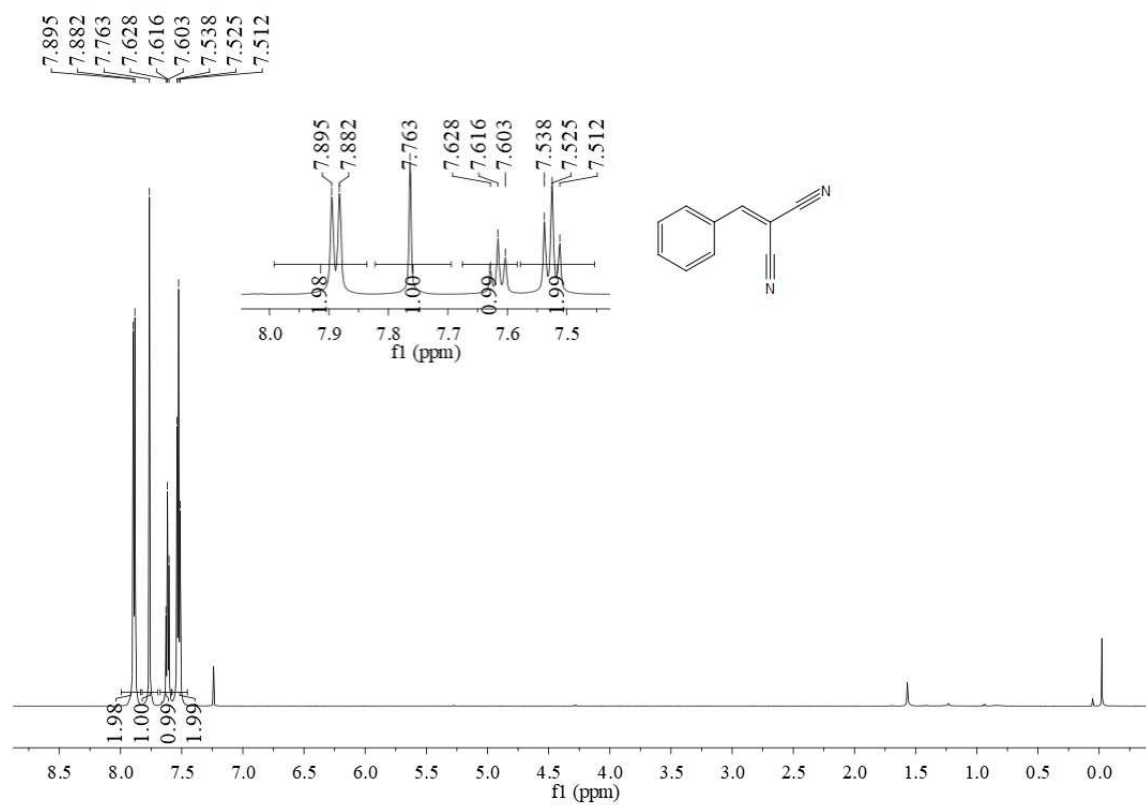


Figure S34. ¹H-NMR spectrum of **2f**.

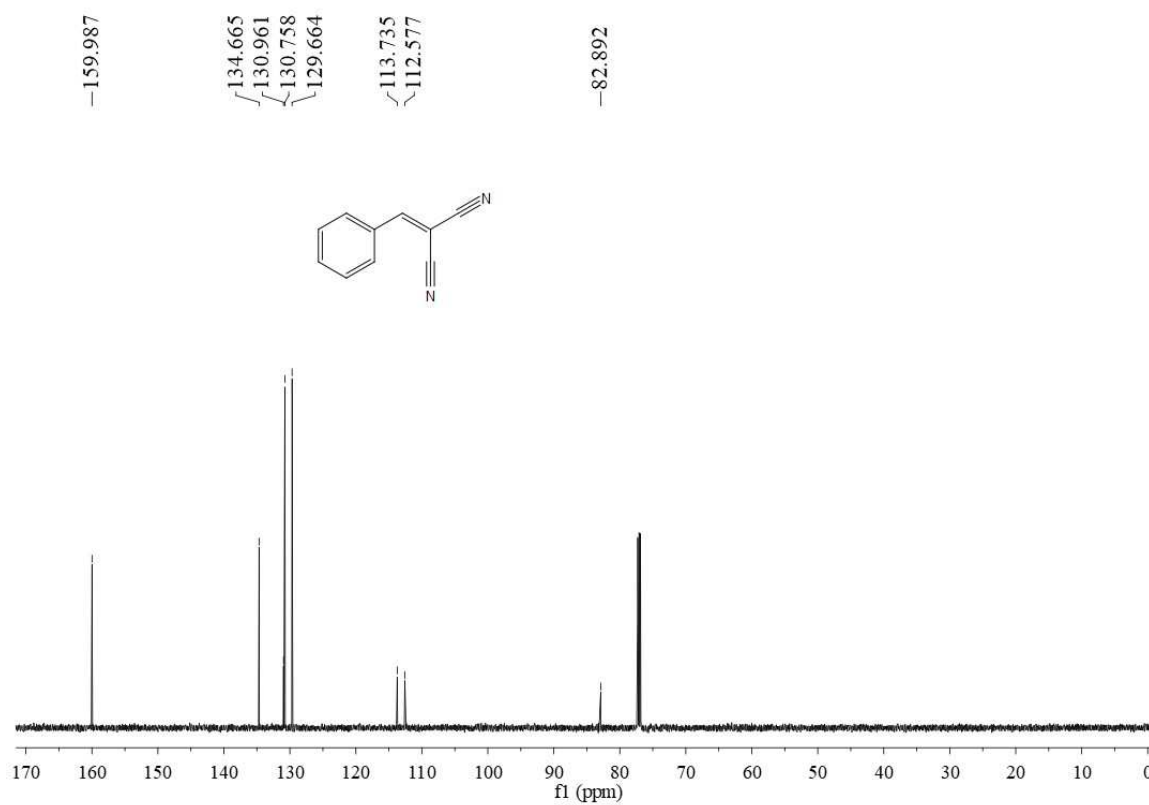


Figure S35. ¹³C-NMR spectrum of **2f**.

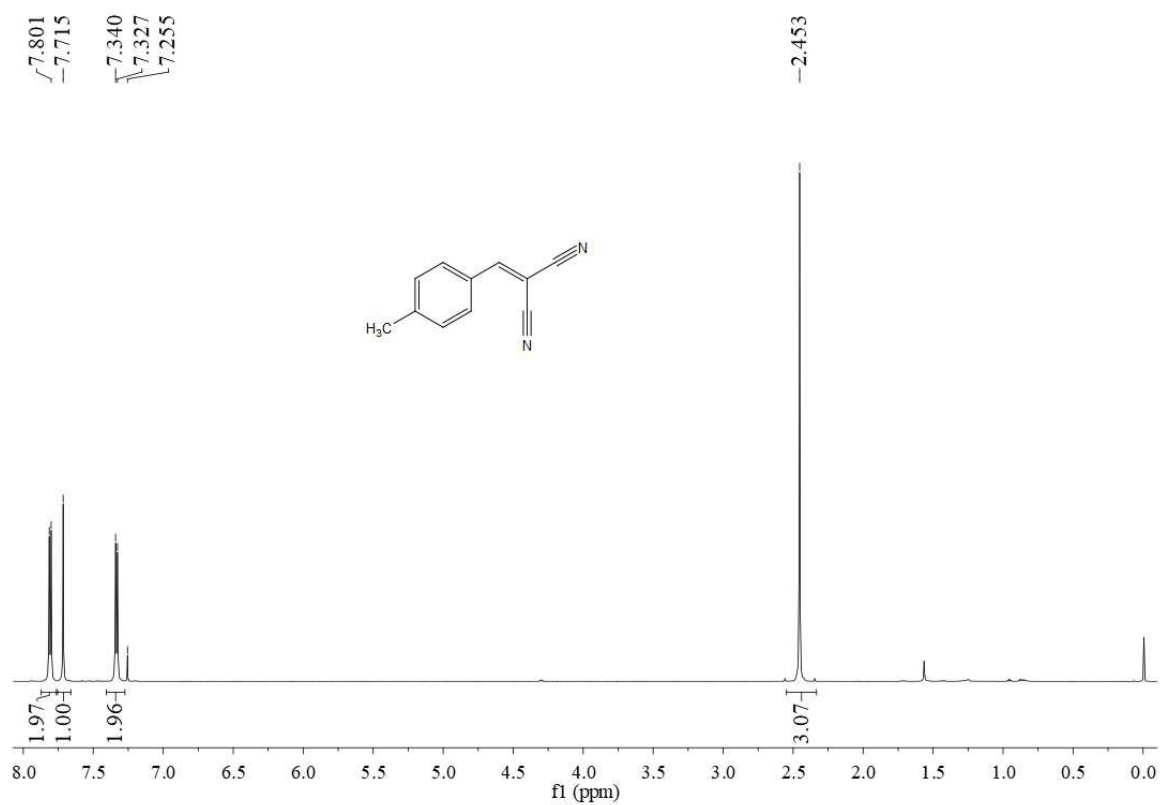


Figure S36. ¹H-NMR spectrum of **2g**.

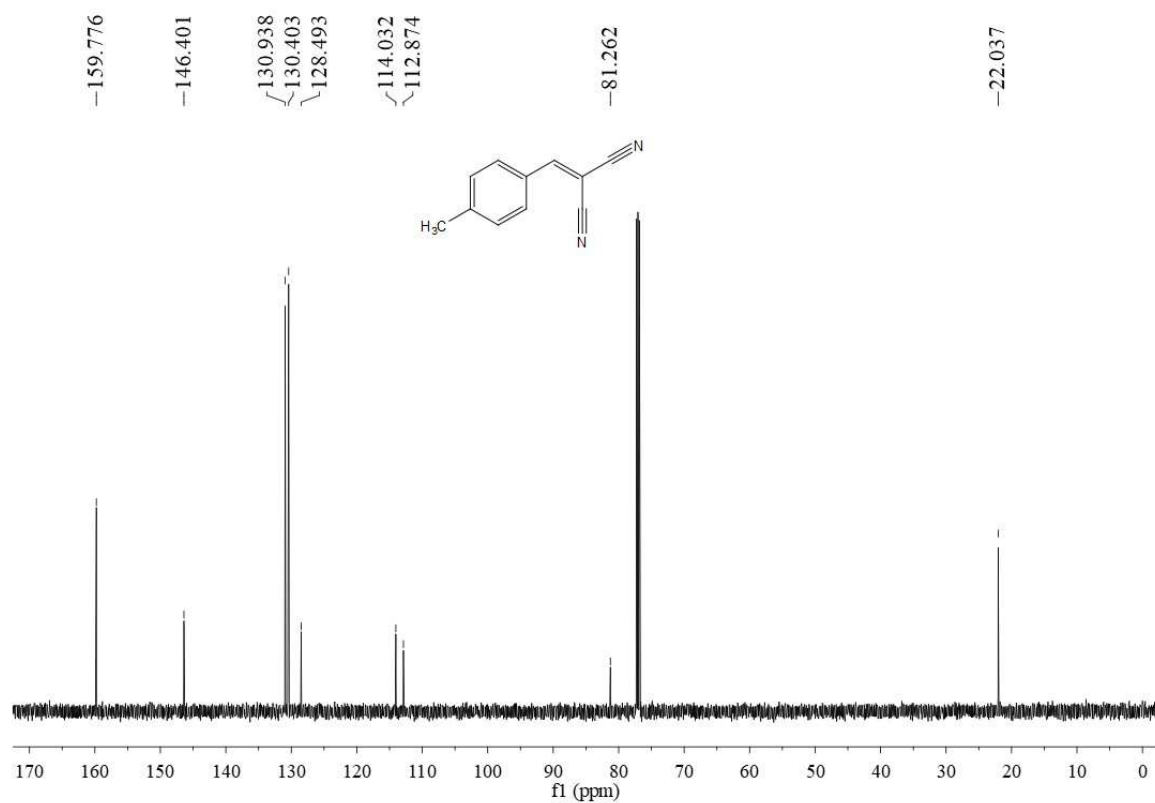


Figure S37. ¹³C-NMR spectrum of **2g**.

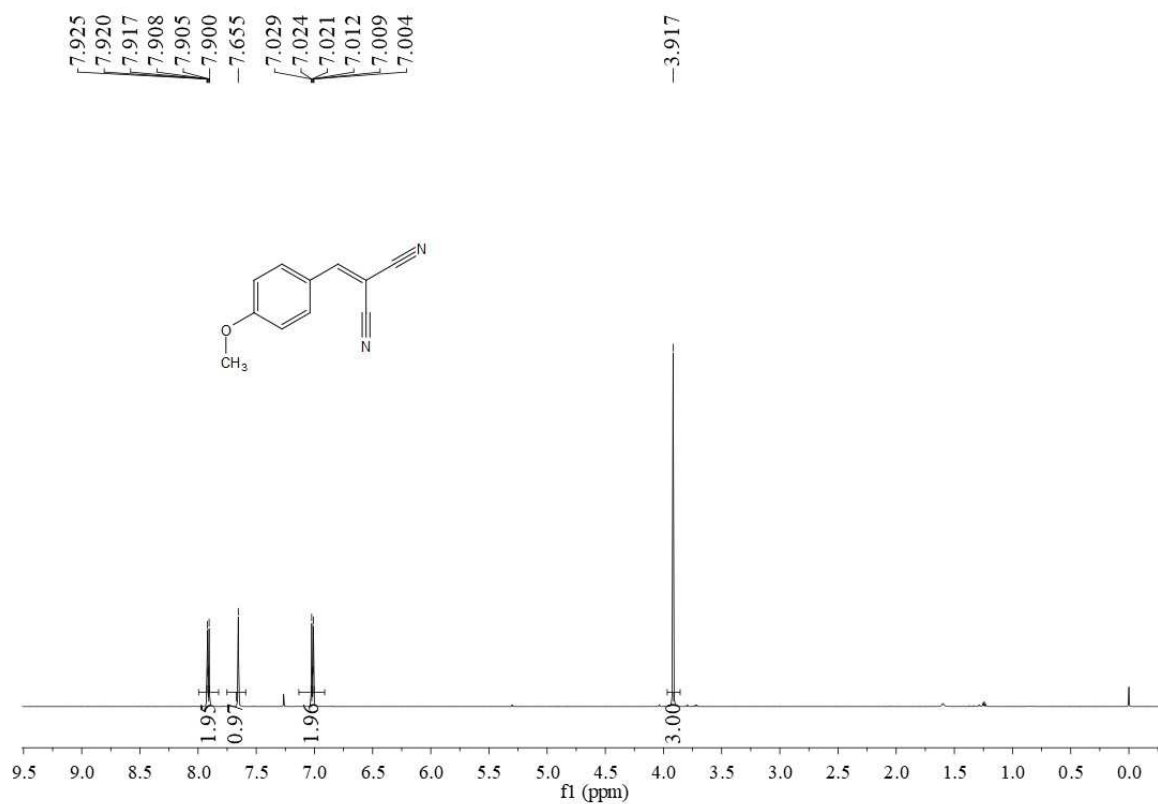


Figure S38. ¹H-NMR spectrum of **2h**.

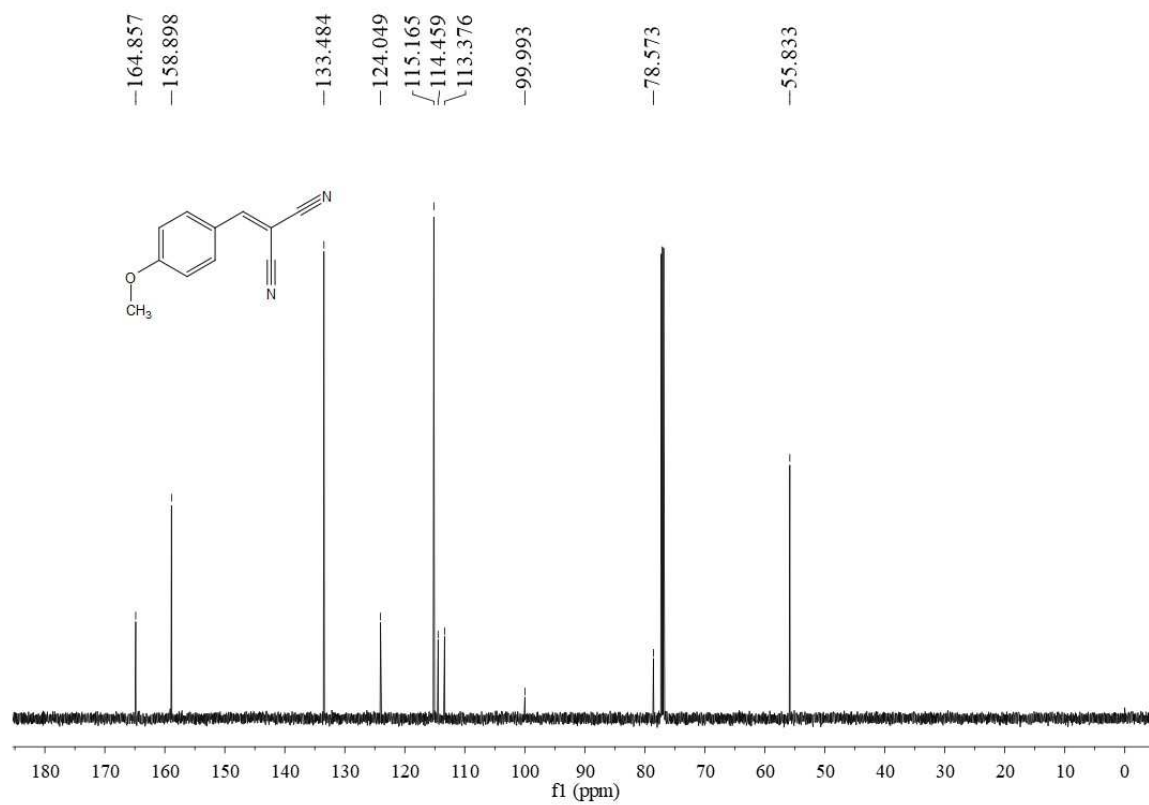


Figure S39. ¹³C-NMR spectrum of **2h**.

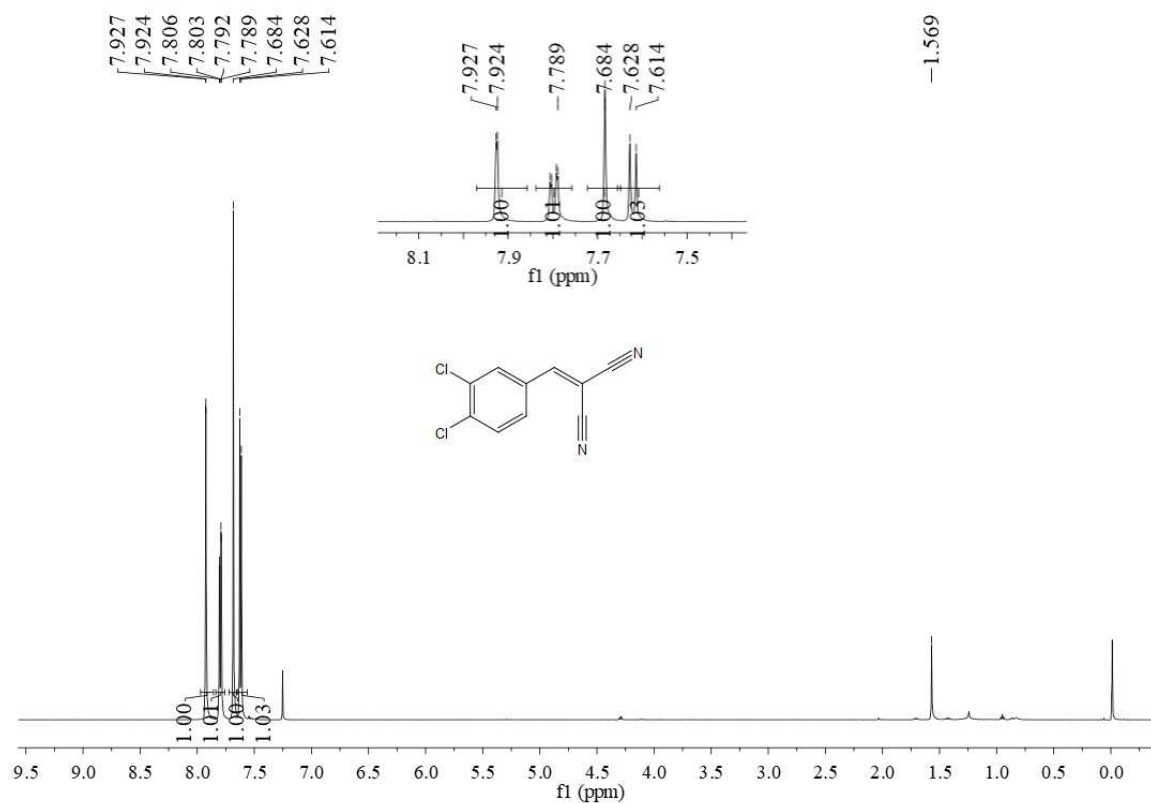


Figure S40. ¹H-NMR spectrum of **2i**.

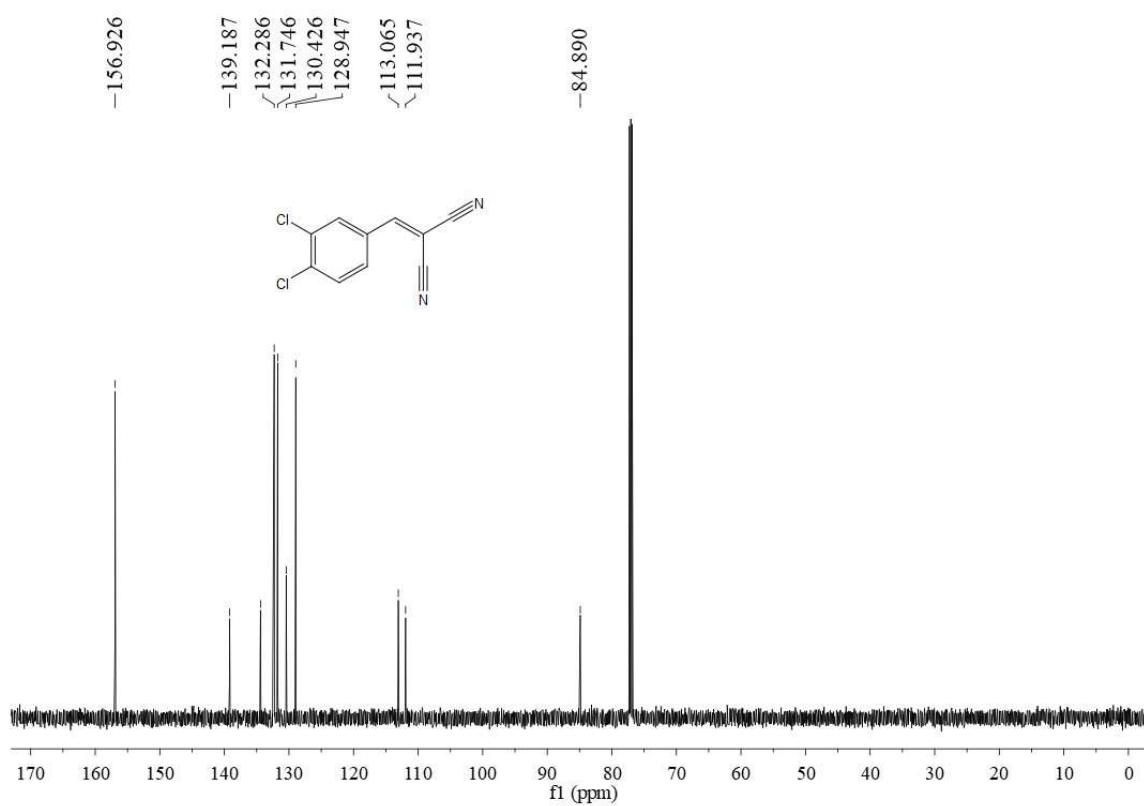


Figure S41. ¹³C-NMR spectrum of **2i**.

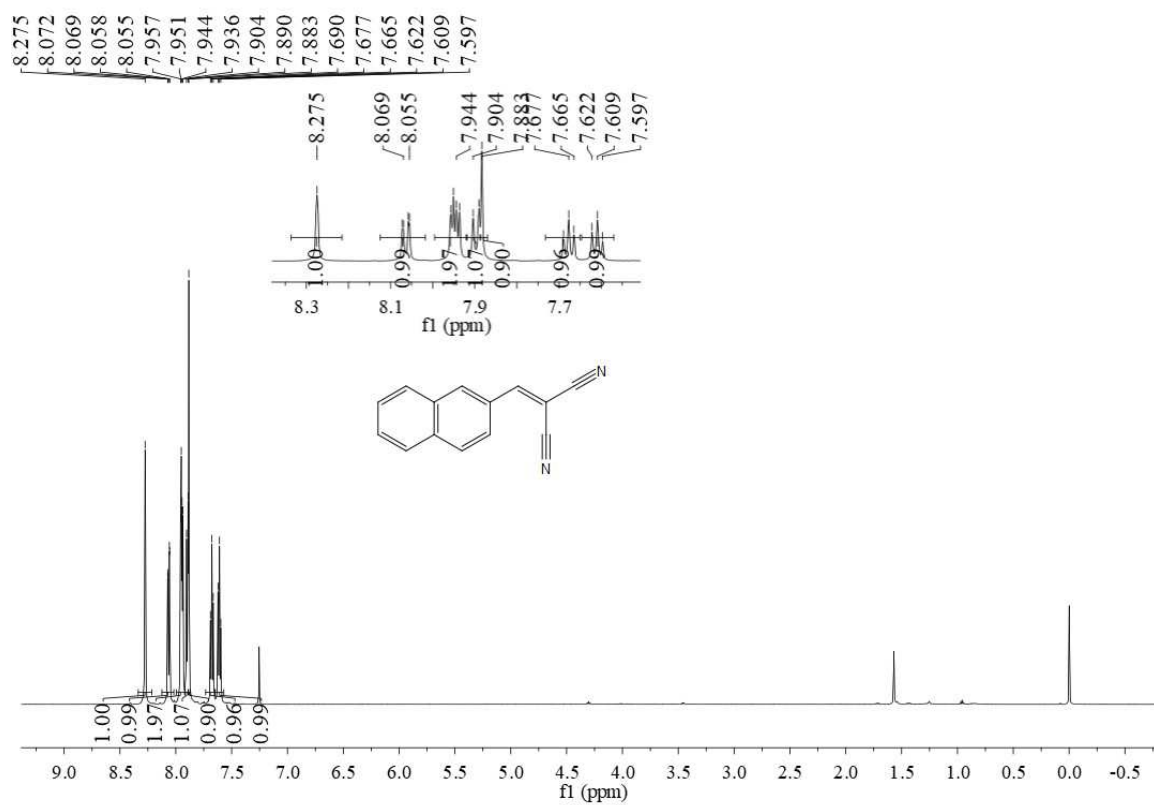


Figure S42. ¹H-NMR spectrum of **2j**.

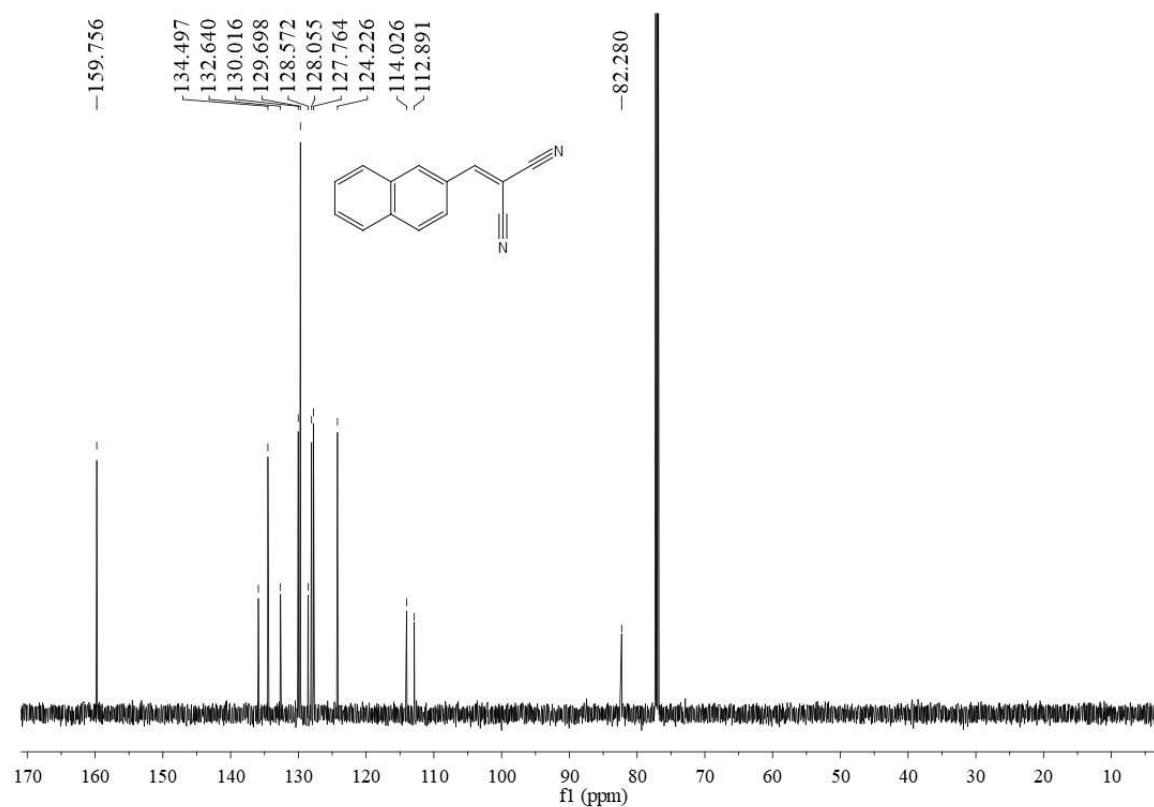


Figure S43. ¹³C-NMR spectrum of **2j**.

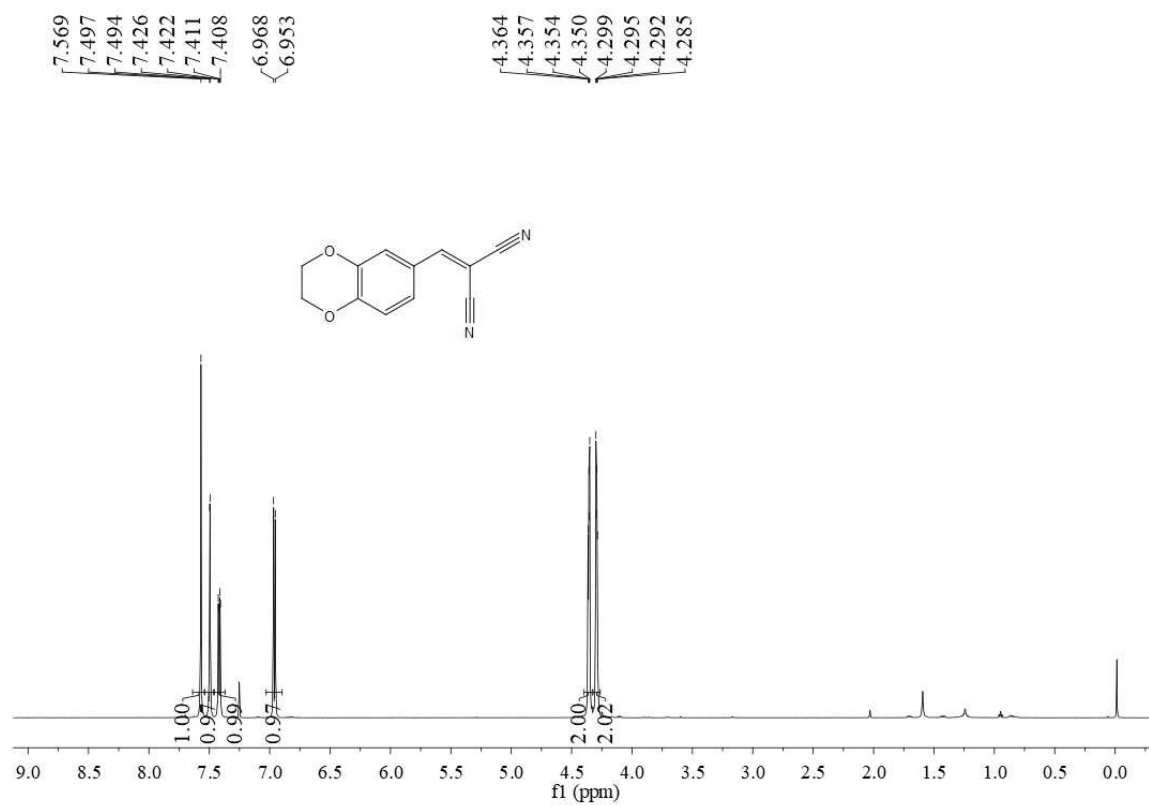


Figure S44. ¹H-NMR spectrum of 2k.

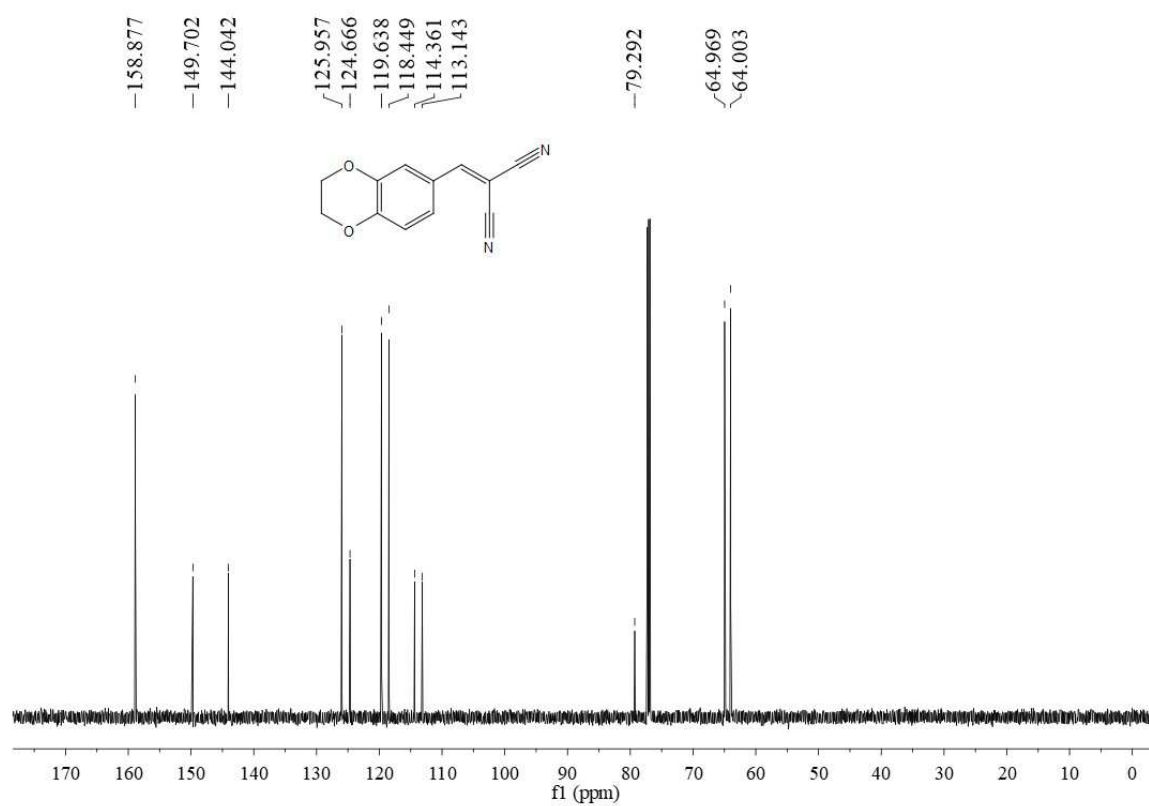


Figure S45. ¹³C-NMR spectrum of 2k.

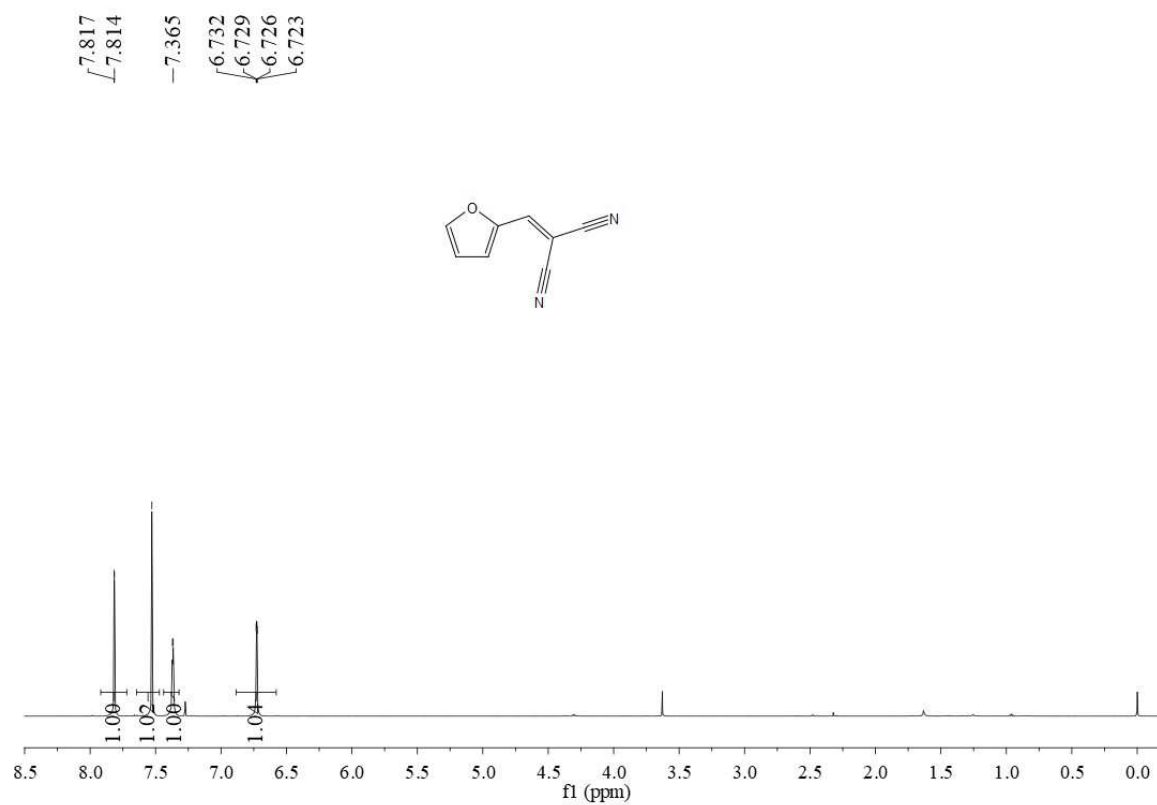


Figure S46. ¹H-NMR spectrum of 2l.

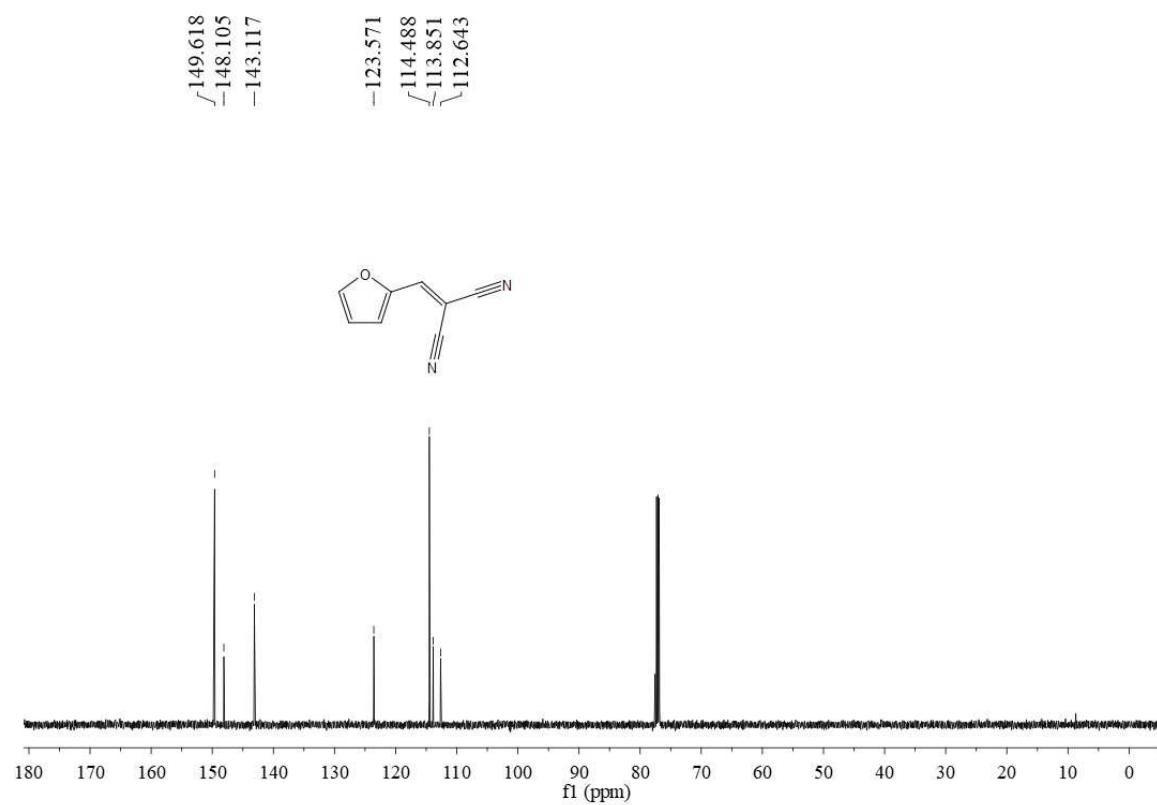


Figure S47. ¹³C-NMR spectrum of 2l.

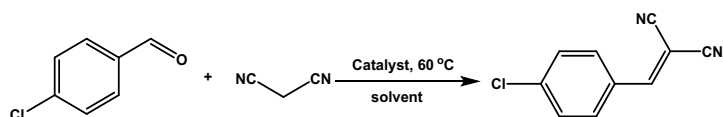
Section C. Supporting Tables

Table S1. Optimization of synthesis conditions for TP-TU-COF

Entry	Solvents	Temperature (°C)	Crystallinity
1	NMP/TCB=2/3	90	No
2	NMP/TCB=1/4	90	No
3	<i>n</i> -BuOH/TCB=1:1	90	No
4	NMP/TCB=2/3	120	Low
5	NMP/TCB=1/4	120	No
6	NMP/TCB=3/2	180	Low
7	NMP/TCB=3/2	120	Moderate
8	NMP/TCB=3/2	150	High

Table S2. Elemental analysis of TP-TU-COF, TP-DMTU-COF, and TP-DMPTU-COF.

		C (%)	H (%)	N (%)	S (%)
TP-TU-COF	Calcd.	56.07	4.67	13.08	14.95
	Found	55.87	4.72	12.94	14.23
TP-DMTU-COF	Calcd.	57.89	5.26	12.28	14.04
	Found	57.21	4.92	11.83	13.76
TP-DMPTU-COF	Calcd.	62.92	5.62	10.49	11.99
	Found	62.13	5.27	10.02	11.28

Table S3. Screening of the reaction conditions ^[a].

entry	catalyst	solvent	yield (%) ^[b]
1	no	toluene	trace
2	TP-DMPTU-COF	toluene	89%
3	TP-DMPTU-COF	THF	40%
4	TP-DMPTU-COF	acetonitrile	52%
5	TP-DMPTU-COF	1, 4-dioxane	63%
6	TP-DMPTU-COF	DCE	47%
7	TP-DMPTU-COF	DMF	78%
8 ^c	TP-DMPTU-COF	toluene: H ₂ O	98%
9 ^c	TP-DMTU-COF	toluene: H ₂ O	95%
10 ^c	TP-TU-COF	toluene: H ₂ O	97%

[a] Unless otherwise noted, the reaction was performed with 2 mol % of catalyst (TP-DMPTU-COF: 7.8 mg; TP-DMTU-COF: 7.0 mg; TP-TU-COF: 6.2 mg), aldehydes (0.3 mmol) and malononitrile (0.45 mmol, 1.5 equiv) in solvent (2.0 mL) at 60 °C for 10 h. [b] Yield of the isolated product. [c] toluene: H₂O = 5:1 (2 ml: 0.4 ml).

Table S4. Atomistic coordinates for the AA-stacking mode of TP-TU-COF optimized using DFTB+ method. Lattice type: hexagonal, Space group: P6/M; $\alpha = \beta = 90^\circ$, $\gamma = 120^\circ$, $a = 21.7621 \text{ \AA}$, $b = 21.7621 \text{ \AA}$, $c = 3.4854 \text{ \AA}$.

C1	C	0.74257	-0.63919	0.5	0	Uiso	1
C2	C	0.71546	-0.58909	0.5	0	Uiso	1
C3	C	0.75692	-0.5181	0.5	0	Uiso	1
N4	N	0.83166	-0.4859	0.5	0	Uiso	1
C5	C	0.88517	-0.41281	0.5	0	Uiso	1
N6	N	0.95808	-0.39506	0.5	0	Uiso	1
S7	S	0.86743	-0.3576	0.5	0	Uiso	1
C8	C	0.98005	-0.44739	0.5	0	Uiso	1
C9	C	0.93143	-0.5198	0.5	0	Uiso	1
C10	C	0.95032	-0.57234	0.5	0	Uiso	1
O11	O	0.80515	-0.61798	0.5	0	Uiso	1
H12	H	0.73188	-0.48294	0.5	0	Uiso	1
H13	H	0.85695	-0.51931	0.5	0	Uiso	1
H14	H	1.00081	-0.33859	0.5	0	Uiso	1
H15	H	0.87209	-0.5393	0.5	0	Uiso	1
H16	H	0.90738	-0.63071	0.5	0	Uiso	1

Table S5. Atomistic coordinates for the AB-stacking mode of TP-TU-COF optimized using DFTB+ method. Lattice type: hexagonal, Space group: P63/M; $\alpha = \beta = 90^\circ$, $\gamma = 120^\circ$, a = 21.7621 Å, b = 21.7621 Å, c = 6.9709 Å.

C1	C	1.07591	1.02748	0.25	0	Uiso	1
C2	C	1.0488	1.07758	0.25	0	Uiso	1
C3	C	1.09026	1.14857	0.25	0	Uiso	1
N4	N	1.16499	1.18077	0.25	0	Uiso	1
C5	C	1.21851	1.25386	0.25	0	Uiso	1
N6	N	1.29142	1.27161	0.25	0	Uiso	1
S7	S	1.20076	1.30907	0.25	0	Uiso	1
C8	C	1.31338	1.21928	0.25	0	Uiso	1
C9	C	1.26476	1.14687	0.25	0	Uiso	1
C10	C	1.28365	1.09432	0.25	0	Uiso	1
O11	O	1.13849	1.04869	0.25	0	Uiso	1
H12	H	1.06521	1.18373	0.25	0	Uiso	1
H13	H	1.19028	1.14735	0.25	0	Uiso	1
H14	H	0.33414	1.32808	0.25	0	Uiso	1
H15	H	1.20542	1.12737	0.25	0	Uiso	1
H16	H	1.24072	1.03596	0.25	0	Uiso	1
C17	C	0.59076	1.30586	0.25	0	Uiso	1
C18	C	0.61787	1.25575	0.25	0	Uiso	1
C19	C	0.57641	1.18476	0.25	0	Uiso	1
N20	N	0.50168	1.15257	0.25	0	Uiso	1
C21	C	0.44816	1.07947	0.25	0	Uiso	1
N22	N	0.37525	1.06173	0.25	0	Uiso	1
S23	S	0.46591	1.02426	0.25	0	Uiso	1
C24	C	0.35329	1.11406	0.25	0	Uiso	1
C25	C	0.40191	1.18647	0.25	0	Uiso	1
C26	C	0.38302	1.23901	0.25	0	Uiso	1
O27	O	0.52818	1.28465	0.25	0	Uiso	1
H28	H	0.60146	1.1496	0.25	0	Uiso	1
H29	H	0.47638	1.18598	0.25	0	Uiso	1
H30	H	1.33252	1.00526	0.25	0	Uiso	1
H31	H	0.46124	1.20596	0.25	0	Uiso	1
H32	H	0.42595	1.29738	0.25	0	Uiso	1

Table S6. Atomistic coordinates for the AA-stacking mode of TP-DMTU-COF optimized using DFTB⁺ method. Lattice type: hexagonal, Space group: P6; $\alpha = \beta = 90^\circ$, $\gamma = 120^\circ$, a = 21.8507 Å, b = 21.8507 Å, c = 3.5805 Å.

C1	C	0.74263	0.36735	0.234	0	Uiso	1
C2	C	0.70892	0.41051	0.28603	0	Uiso	1
C3	C	0.74531	0.47991	0.35391	0	Uiso	1
N4	N	0.8139	0.51237	0.51745	0	Uiso	1
C5	C	0.87311	0.57596	0.39347	0	Uiso	1
N6	N	0.94212	0.59285	0.51707	0	Uiso	1
S7	S	0.86267	0.63118	0.2442	0	Uiso	1
C8	C	0.97026	0.54523	0.55565	0	Uiso	1
C9	C	0.92803	0.4713	0.57576	0	Uiso	1
C10	C	0.9567	0.42652	0.59777	0	Uiso	1
O11	O	0.80238	0.39344	0.11315	0	Uiso	1
C12	C	0.08971	0.64969	0.70895	0	Uiso	1
H13	H	0.72046	0.51114	0.31562	0	Uiso	1
H14	H	0.97713	0.64702	0.53551	0	Uiso	1
H15	H	0.87297	0.44704	0.59588	0	Uiso	1
H16	H	0.81842	0.49472	0.77808	0	Uiso	1
H17	H	0.09842	0.68728	0.48359	0	Uiso	1
H18	H	0.14154	0.66018	0.81252	0	Uiso	1
H19	H	0.06322	0.66206	0.93317	0	Uiso	1

Table S7. Atomistic coordinates for the AB-stacking mode of TP-DMTU-COF optimized using DFTB⁺ method. Lattice type: hexagonal, Space group: P63; $\alpha = \beta = 90^\circ$, $\gamma = 120^\circ$, a = 21.8507 Å, b = 21.8507 Å, c = 7.1610 Å.

C1	C	1.07597	0.03402	0.117	0	Uiso	1
C2	C	1.04225	0.07718	0.14302	0	Uiso	1
C3	C	1.07864	0.14658	0.17696	0	Uiso	1
N4	N	1.14724	0.17904	0.25872	0	Uiso	1
C5	C	1.20644	0.24263	0.19674	0	Uiso	1
N6	N	1.27545	0.25952	0.25854	0	Uiso	1
S7	S	1.196	0.29785	0.1221	0	Uiso	1
C8	C	1.30359	0.21189	0.27782	0	Uiso	1
C9	C	1.26136	0.13797	0.28788	0	Uiso	1
C10	C	1.29003	0.09318	0.29889	0	Uiso	1
O11	O	1.13572	0.06011	0.05657	0	Uiso	1
C12	C	0.42305	0.31635	0.35447	0	Uiso	1
H13	H	1.05379	0.17781	0.15781	0	Uiso	1
H14	H	1.31046	0.31369	0.26775	0	Uiso	1
H15	H	1.2063	0.11371	0.29794	0	Uiso	1
H16	H	1.15176	0.16139	0.38904	0	Uiso	1
H17	H	0.43176	0.35395	0.24179	0	Uiso	1
H18	H	0.47487	0.32684	0.40626	0	Uiso	1
H19	H	0.39656	0.32873	0.46659	0	Uiso	1
C20	C	0.5907	0.29931	0.117	0	Uiso	1
C21	C	0.62441	0.25615	0.14302	0	Uiso	1
C22	C	0.58802	0.18675	0.17696	0	Uiso	1
N23	N	0.51943	0.15429	0.25872	0	Uiso	1
C24	C	0.46023	0.09071	0.19674	0	Uiso	1
N25	N	0.39121	0.07381	0.25854	0	Uiso	1
S26	S	0.47067	0.03548	0.1221	0	Uiso	1
C27	C	0.36307	0.12144	0.27782	0	Uiso	1
C28	C	0.40531	0.19536	0.28788	0	Uiso	1
C29	C	0.37664	0.24015	0.29889	0	Uiso	1
O30	O	0.53095	0.27323	0.05657	0	Uiso	1
C31	C	1.24362	0.01698	0.35447	0	Uiso	1
H32	H	0.61287	0.15552	0.15781	0	Uiso	1
H33	H	0.35621	0.01964	0.26775	0	Uiso	1
H34	H	0.46036	0.21963	0.29794	0	Uiso	1
H35	H	0.51491	0.17194	0.38904	0	Uiso	1
H36	H	1.23491	0.02061	0.24179	0	Uiso	1

H37	H	1.1918	0.00649	0.40626	0	Uiso	1
H38	H	1.27011	0.0046	0.46659	0	Uiso	1

Table S8. Atomistic coordinates for the AA-stacking mode of TP-DMPTU-COF optimized using DFTB⁺ method. Lattice type: hexagonal, Space group: P6; $\alpha = \beta = 90^\circ$, $\gamma = 120^\circ$, a = 28.6367 Å, b = 28.6367 Å, c = 3.6239 Å.

C1	C	-0.36821	0.35731	0.55747	0	Uiso	1
C2	C	-0.30909	0.39303	0.60294	0	Uiso	1
C3	C	-0.28352	0.44679	0.6667	0	Uiso	1
N4	N	-0.30621	0.48215	0.64572	0	Uiso	1
C5	C	-0.27712	0.53427	0.46332	0	Uiso	1
N6	N	-0.30174	0.56714	0.41667	0	Uiso	1
S7	S	-0.22058	0.55786	0.37425	0	Uiso	1
C8	C	-0.35874	0.54701	0.41227	0	Uiso	1
C9	C	-0.39353	0.49546	0.28387	0	Uiso	1
C10	C	-0.44909	0.47646	0.24904	0	Uiso	1
C11	C	-0.47042	0.51006	0.34371	0	Uiso	1
C12	C	-0.43505	0.56219	0.47359	0	Uiso	1
C13	C	-0.37967	0.58092	0.50914	0	Uiso	1
O14	O	-0.39716	0.37494	0.45482	0	Uiso	1
H15	H	-0.24069	0.46589	0.7149	0	Uiso	1
H16	H	-0.34421	0.47019	0.75909	0	Uiso	1
H17	H	-0.27635	0.6072	0.35187	0	Uiso	1
H18	H	-0.37342	0.46879	0.23871	0	Uiso	1
H19	H	-0.47486	0.43554	0.15159	0	Uiso	1
H20	H	-0.45106	0.5876	0.56025	0	Uiso	1
C21	C	-0.34369	0.63648	0.66252	0	Uiso	1
H22	H	-0.36747	0.65181	0.80775	0	Uiso	1
H23	H	-0.32021	0.66487	0.43981	0	Uiso	1
H24	H	-0.3153	0.63448	0.86	0	Uiso	1

Table S9. Atomistic coordinates for the AB-stacking mode of TP-DMPTU-COF optimized using DFTB⁺ method. Lattice type: hexagonal, Space group: P63; $\alpha = \beta = 90^\circ$, $\gamma = 120^\circ$, a = 28.6367 Å, b = 28.6367 Å, c = 7.2478 Å.

C1	C	0.9649	0.02372	0.27874	0	Uiso	1
C2	C	1.02398	0.05966	0.30147	0	Uiso	1
C3	C	1.04933	0.11342	0.33335	0	Uiso	1
N4	N	1.0264	0.14856	0.32286	0	Uiso	1
C5	C	1.05528	0.20069	0.23166	0	Uiso	1
N6	N	1.03041	0.23334	0.20834	0	Uiso	1
S7	S	1.11184	0.22453	0.18712	0	Uiso	1
C8	C	0.97337	0.21296	0.20614	0	Uiso	1
C9	C	0.93877	0.16136	0.14194	0	Uiso	1
C10	C	0.88316	0.14211	0.12452	0	Uiso	1
C11	C	0.86159	0.17551	0.17186	0	Uiso	1
C12	C	0.89678	0.22768	0.23679	0	Uiso	1
C13	C	0.9522	0.24666	0.25457	0	Uiso	1
O14	O	0.93577	0.04114	0.22741	0	Uiso	1
H15	H	1.09218	0.13269	0.35745	0	Uiso	1
H16	H	0.98836	0.13642	0.37955	0	Uiso	1
H17	H	1.05566	0.27343	0.17594	0	Uiso	1
H18	H	0.95907	0.13487	0.11935	0	Uiso	1
H19	H	0.85754	0.10116	0.07579	0	Uiso	1
H20	H	0.88059	0.25294	0.28013	0	Uiso	1
C21	C	0.98797	0.30226	0.33126	0	Uiso	1
H22	H	0.96405	0.31743	0.40387	0	Uiso	1
H23	H	1.01137	0.3307	0.2199	0	Uiso	1
H24	H	1.01645	0.30042	0.43	0	Uiso	1
C25	C	0.70176	0.30961	0.27874	0	Uiso	1
C26	C	0.64269	0.27367	0.30147	0	Uiso	1
C27	C	0.61733	0.21991	0.33335	0	Uiso	1
N28	N	0.64027	0.18478	0.32286	0	Uiso	1
C29	C	0.61138	0.13264	0.23166	0	Uiso	1
N30	N	0.63625	0.09999	0.20834	0	Uiso	1
S31	S	0.55483	0.10881	0.18712	0	Uiso	1
C32	C	0.6933	0.12037	0.20614	0	Uiso	1
C33	C	0.7279	0.17197	0.14194	0	Uiso	1
C34	C	0.78351	0.19122	0.12452	0	Uiso	1
C35	C	0.80508	0.15783	0.17186	0	Uiso	1
C36	C	0.76989	0.10565	0.23679	0	Uiso	1
C37	C	0.71446	0.08667	0.25457	0	Uiso	1

O38	O	0.73089	0.29219	0.22741	0	Uiso	1
H39	H	0.57449	0.20064	0.35745	0	Uiso	1
H40	H	0.67831	0.19691	0.37955	0	Uiso	1
H41	H	0.61101	0.0599	0.17594	0	Uiso	1
H42	H	0.70759	0.19846	0.11935	0	Uiso	1
H43	H	0.80913	0.23217	0.07579	0	Uiso	1
H44	H	0.78608	0.08039	0.28013	0	Uiso	1
C45	C	0.67869	0.03107	0.33126	0	Uiso	1
H46	H	0.70261	0.01591	0.40387	0	Uiso	1
H47	H	0.6553	0.00263	0.2199	0	Uiso	1
H48	H	0.65021	0.03291	0.43	0	Uiso	1

Section D. Supporting References

- [S1] C. R. Deblase, K. E. Silberstein, T. -T. Truong, H. D. Abruña, W. R. Dichtel, *J. Am. Chem. Soc.* **2013**, *135*, 16821-16824.
- [S2] M. Matsumoto, R. R. Dasari, W. Ji, C. H. Feriante, T. C. Parker, S. R. Marder, W. R. Dichtel, *J. Am. Chem. Soc.* **2017**, *139*, 4999-5002.
- [S3] E. Vitaku, W. R. Dichtel, *J. Am. Chem. Soc.* **2017**, *139*, 12911-12914.